TGG-3′ for the NF-κB binding site of Pai-2, 5′-TGAGTGTGAGTGGTGCAG ATTAC-3′ and 5′-CCTCCCACACAGCTCTTTTTTC-3′ for mPai-2 TATA, 5′-CGGAGGGTAGTTCCATGAAA-3′ and 5′-CAGGCTTTTACCCACGCAA A-3′ for the NF-κB binding site of mCox2, and 5′-CGCAACTCACTGAAGC AGAG-3′ and 5′-TCCTTCGTGAGCAGAGTCCT-3′ for mCox-2 TATA. The antibodies used were as follows: anti-AhR serum, preimmune serum, anti-p65, and anti-PolII antibodies (Santa Cruz).

Western blot analyses. Cells were dissolved in SDS sample buffer, and proteins were separated by SDS-PAGE for Western blot analysis. The proteins were then transferred to polyvinylidene difluoride membranes and blocked in 3% skim milk for 30 min. Each antibody was used as a primary reagent, and after being washed three times with Tris-borate-EDTA containing 0.1% Triton X-100, membranes were incubated with species-specific horseradish peroxidase-conjugated secondary antibody (Zymed). The protein-antibody complexes were visualized by using an enhanced chemiluminescence detection system (Amersham) according to the manufacturer's recommendations. Nuclear extracts were prepared by a standard method (25). The antibodies used were as follows: anti-Arnt serum (28); anti-AhR (Biomol); anti-Pai-2, anti-p65, and antilamin antibodies (Santa Cruz); and antitubulin antibody (Sigma).

RESULTS

High susceptibility of AhR-deficient mice to LPS-induced endotoxin shock. To investigate the function of AhR in acute inflammation in vivo, we performed studies of experimental LPS-induced endotoxin shock. For these studies, 10-week-old AhR WT and AhR KO mice were injected intraperitoneally with 20 mg/kg LPS. After 24 h, while all of the AhR WT mice survived, most of the AhR KO mice (80%) had died (Fig. 1A). These data indicate that AhR-deficient mice were highly susceptible to LPS-induced endotoxin shock. To explain the increased sensitivity of AhR KO mice to septic shock, the plasma concentrations of several inflammatory cytokines were measured 2 h after LPS challenge. Consistent with the enhanced susceptibility of AhR KO mice to the LPS treatment, AhR KO mice had marked increases in plasma IL-1β, IL-18, and TNF-α levels ($P < 0.001$), with modest increases in IL-6 and IFN-γ (Fig. 1B). In contrast, there was no difference in plasma IL-12p70 levels (Fig. 1B). Administration of 3MC, an AhR ligand, before LPS treatment (30 mg/kg) made the AhR WT mice significantly more resistant to septic shock than the mice that were not treated with 3MC ($P = 0.002$) (Fig. 1C). Together with the fact that there was essentially no effect of 3MC on AhR KO mice, these results suggested that activated AhR could play an anti-inflammatory role.

Increased susceptibility of mice with AhR KO macrophages to LPS-induced endotoxin shock. Since macrophages play an important role in sensitivity to LPS toxicity, we generated mice with macrophages deficient in AhR ($AhR^{flox/-}$::LysM Cre [ΔAhR Mac] mice) to evaluate the contribution of macrophages to the LPS hypersensitivity of AhR KO mice. When ΔAhR Mac and control mice ($AhR^{flox/-}$) were injected intraperitoneally with 25 mg/kg LPS, most of the ΔAhR Mac mice (80%) had died at 48 h after LPS challenge, while 60% of the control mice survived ($P = 0.03$) (Fig. 2A). Together with the previous results, these data showed that dysfunctional AhR-deficient macrophages are one of the main causes of LPS hypersensitivity in AhR KO mice.

Elevated IL-1β secretion from AhR KO BMDM in response to LPS. To further investigate the cause of the aberrant cytokine secretion by LPS-challenged AhR KO mice, we next asked if there were any differences in the production of proinflammatory cytokines by AhR WT and AhR KO mouse

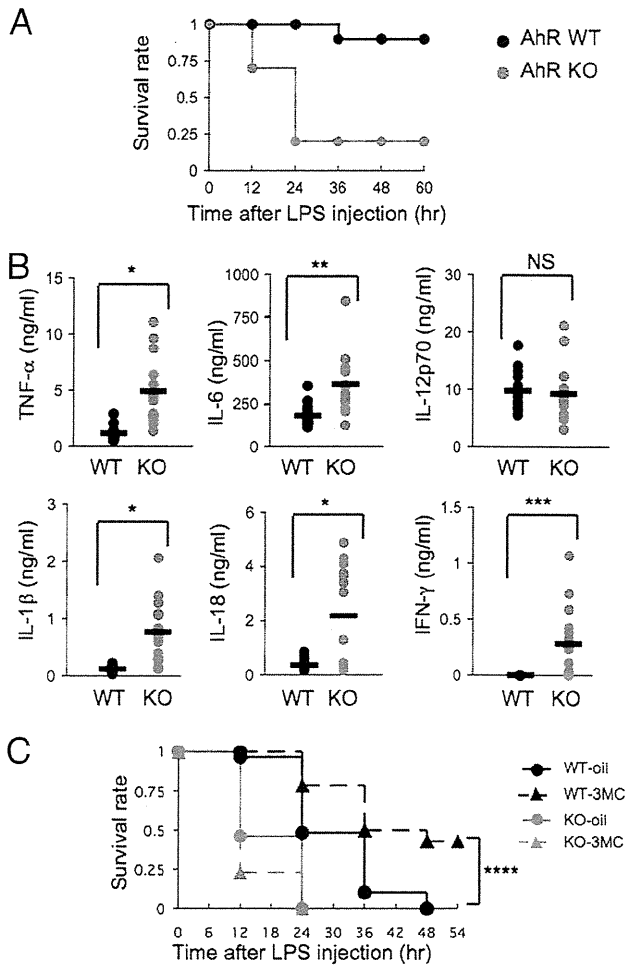

FIG. 1. High susceptibility of AhR KO mice to LPS-induced endotoxin shock. (A) Survival of AhR WT and AhR KO mice ($n = 10$) after LPS challenge (20 mg/ml). (B) TNF-α, IL-6, IL-12p70, IL-1β, IL-18, and IFN-γ plasma levels 2 h after LPS challenge (20 mg/ml). Horizontal bars show the mean results. (C) Partial protection of AhR WT mice from septic shock by intraperitoneal injection of 3MC at 2 h before LPS challenge (30 mg/ml) and survival of corn oil-injected mice. AhR WT-oil, $n = 29$; AhR WT-3MC, $n = 28$; AhR KO-oil, $n = 13$; AhR KO-3MC, $n = 13$. *, $P < 0.001$; **, $P = 0.001$; ***, $P < 0.005$; ****, $P = 0.002$; NS, not significant.

BMDM in response to LPS stimulation. Macrophages from the bone marrow of AhR WT and AhR KO mice were challenged with 10 ng/ml LPS for 8 h, and then the levels of TNF-α and IL-1β in the culture medium were assessed by ELISA. Compared to the levels in AhR WT BMDM, the levels of IL-1β secretion by AhR KO BMDM were markedly elevated, along with slight increases in TNF-α, in response to LPS treatment ($P < 0.001$) (Fig. 2B, left). However, IL-1β mRNA levels were not altered between AhR WT and AhR KO BMDM (Fig. 2C, left). These data indicated that AhR deficiency markedly increased IL-1β accumulation due to its enhanced secretion rather than its increased synthesis.

Expression of AhR-dependent genes in macrophages. We next performed microarray analysis of AhR WT and AhR KO mouse macrophages to comprehensively investigate the AhR-

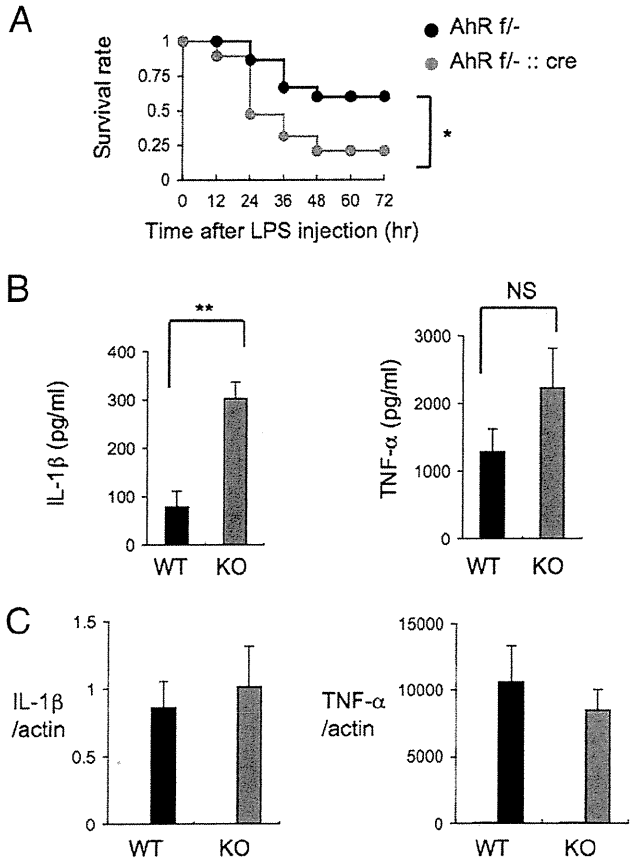

FIG. 2. LPS induces abnormal secretion of IL-1β by BMDM from AhR KO mice. (A) Survival of $AhR^{flox/-}$ (AhR f/−; $n = 15$) and $AhR^{flox/-}$::LysM Cre (AhR f/−::cre; $n = 19$) mice after LPS challenge (25 mg/ml). (B) IL-1β and TNF-α levels in the culture supernatants of AhR WT and AhR KO BMDM 8 h after LPS stimulation (10 ng/ml) ($n = 4$). (C) Relative expression levels of IL-1β and TNF-α mRNA 4 h after LPS stimulation (10 ng/ml) of AhR WT and AhR KO BMDM. Gray and black bars show results with LPS; white bars show results for untreated cells. Error bars show standard deviations. *, $P = 0.03$; **, $P < 0.001$; NS, not significant.

dependent changes in gene expression that were related to IL-1β secretion (Table 1). Among the genes whose expression was reduced in AhR KO macrophages, we noted the markedly reduced levels of expression of the Pai-2 and Bcl-2 genes. These genes were significant because they had been reported to negatively regulate IL-1β secretion by inhibiting the activity of caspase-1 (5, 10). Consistent with the notion that the enhanced secretion of IL-1β is due to the activation of caspase-1, treatment with the caspase inhibitors Z-YVAD-FMK and Z-VAD-FMK markedly reduced the secretion of IL-1β in AhR KO BMDM (Fig. 3A). To confirm their reduced expression in AhR KO BMDM, Pai-2 and Bcl-2 mRNA expression levels were determined by real-time RT-PCR in AhR WT and AhR KO BMDM (Fig. 3B). Figure 3B shows that Pai-2 and Bcl-2 mRNA expression levels were clearly reduced in AhR KO BMDM. To investigate whether the increased IL-1β secretion in AhR KO BMDM was due to their reduced Pai-2 and Bcl-2 expression, the expression of these proteins was supplemented in AhR KO BMDM by infection with adenoviral vectors expressing hPai-2 and hBcl-2 (Fig. 3D). The efficiency of the adenoviral gene transfer, as monitored by the expression of GFP, was estimated to be >90% (data not shown). Compared with control adenoviral expression of GFP, transfer of the hPai-2 gene into AhR KO BMDM significantly inhibited LPS-induced secretion of IL-1β (Fig. 3C), but almost no effect was observed with Bcl-2 expression. Bcl-2 has been reported to suppress IL-1β secretion that is specifically processed through the NALP1 complex and regulated by muramyl dipeptide, which is usually a contaminant in commercial LPS (5). These results suggested that the enhanced IL-1β secretion in response to LPS was due not to processing through the NALP1 complex (5) but to processing through the NALP3 complex, an inflammasome-containing caspase-1 regulated by LPS (16), and that decreased Pai-2 expression is at least one of the causes for the increased IL-1β secretion by AhR KO BMDM after LPS treatment.

Arnt is not required for enhancement of LPS-induced Pai-2 expression by AhR. It has been reported that LPS stimulation induces Pai-2 expression (21, 26). Figure 4A and B show that the induction of both Pai-2 mRNA and protein expression was remarkably reduced in AhR KO macrophages compared with the levels in AhR WT macrophages. Interestingly, AhR mRNA and protein expression levels were also induced by LPS stimulation (Fig. 4A and B). In response to various PAHs, AhR is known to act, in most cases, as a transcriptional activator, in heterodimer formation with Arnt. Although the mouse Pai-2 promoter does not have any obvious XRE sequences (GCGTG) in its regions 5 kb upstream and down-

TABLE 1. Decreased gene expression in AhR KO PEMs revealed by cDNA microarray analysis

Fold change	Value for		Gene name	Gene product
	WT PEMs	KO PEMs		
14.0	0.561	0.040	*Gsta3*	Glutathione *S*-transferase alpha 3
10.2	7.826	0.767	*Pai-2*	Plasminogen activator inhibitor-2
5.5	9.354	1.700	*Cyp1b1*	Cytochrome P450, family 1, subfamily b, polypeptide 1
4.6	0.206	0.045	*Nkrf*	NF-κB repressing factor
3.6	1.922	0.541	*Cxcl5*	Chemokine (C-X-C motif) ligand 5
3.1	13.670	4.444	*Mmp8*	Matrix metallopeptidase 8
2.9	1.406	0.489	*Cxcl13*	Chemokine (C-X-C motif) ligand 13
2.6	2.111	0.800	*Lrrc27*	Leucine-rich repeat-containing 27
2.5	3.466434	1.394728	*Ctgf*	Connective tissue growth factor
2.2	3.849141	1.722473	*Mcoln3*	Mucolipin 3
2.2	1.204793	0.550093	*Nqo1*	NAD(P)H dehydrogenase, quinone 1
2.0	6.96623	3.453017	*Ier3*	Immediate early response 3
2.0	0.596479	0.294062	*Bcl2*	B-cell leukemia/lymphoma 2

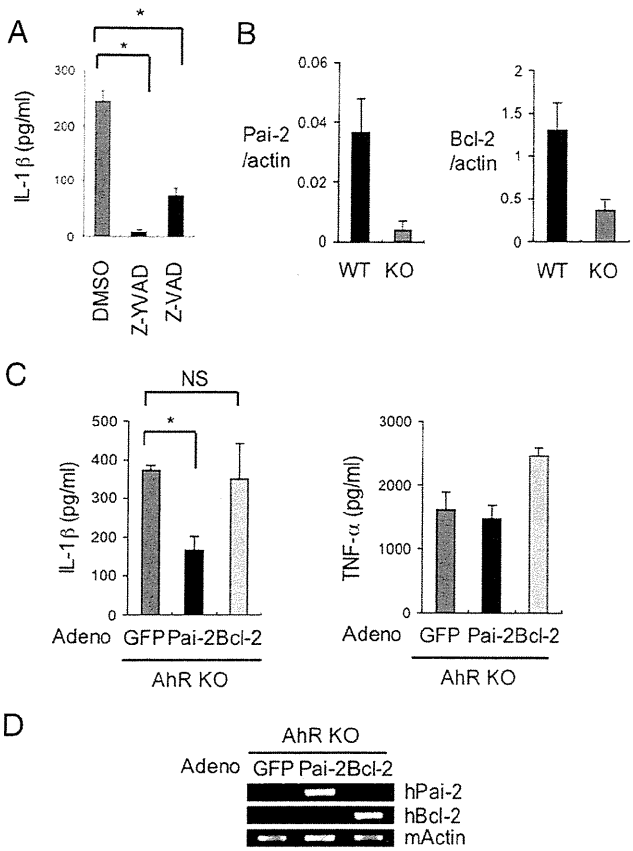

FIG. 3. Decreased Pai-2 expression is one of the causes of the increased IL-1β secretion by LPS-treated AhR KO BMDM. (A) Inhibition of IL-1β oversecretion from AhR KO BMDM by treatment with caspase-1 inhibitor (Z-YVAD-FMK) or caspase inhibitor (Z-VAD-FMK). (B) Relative expression levels of Pai-2 and Bcl-2 mRNA in AhR WT and AhR KO BMDM. (C) The effect of hPai-2 and hBcl-2 reconstitution on the LPS-induced secretion of IL-1β and TNF-α by AhR KO BMDM. BMDM from AhR KO mice were infected with the individual adenovirus (adeno) vectors and then washed and incubated for 24 h. IL-1β and TNF-α levels in the supernatants 8 h after LPS stimulation ($n = 3$) were determined by ELISA. (D) Assessment of hPai-2 and hBcl-2 mRNA expression in adenovirus (adeno) vector-infected BMDM by conventional RT-PCR. Error bars show standard deviations. *, $P < 0.001$; NS, not significant.

stream of the transcription start site, we were interested in determining whether Arnt was also involved in the inducible expression of Pai-2 by LPS. Other AhR target genes identified by the microarray analysis, e.g., the matrix metalloproteinase (Mmp-8) gene and the NAD(P)H:quinone oxidoreductase 1 (Nqo1) gene (Table 1), have characteristic XRE sequences in their promoter regions and were also induced by 3MC. As expected, the induction of their expression was greatly reduced in Arnt KO and Arnt small interfering RNA (siRNA)-treated macrophages (Fig. 4E; also see Fig. S1 in the supplemental material). In stark contrast, the expression of Pai-2 was not much different in Arnt KO and Arnt siRNA-treated macrophages, indicating that Arnt is not involved in regulating Pai-2 gene expression (Fig. 4D; also see Fig. S1 in the supplemental material) and that AhR regulates Pai-2 gene expression by a noncanonical mechanism. Consistent with these observations, macrophage-specific conditional deletion of Arnt did not significantly alter the sensitivity to LPS treatment (Fig. 4F).

DNA elements regulating Pai-2 gene expression. We were interested in further investigating how AhR regulates Pai-2 gene expression in macrophages. It has been previously reported that LPS-induced Pai-2 expression requires NF-κB activation (21) and that AhR and p65 physically interact with each other (31). With those results in mind, we constructed a reporter gene by fusing a 2.7-kb sequence upstream of the mouse Pai-2 transcription start site to the luciferase gene (see Fig. S2 in the supplemental material). This 2.7-kb Pai-2 reporter gene contained a previously reported NF-κB site (21). When the AhR expression vector alone was transfected into RAW 264.7 cells, it did not enhance LPS-induced reporter gene expression. In contrast, cotransfection of both AhR and p65 did (Fig. 5A). To identify the sequence responsible for enhancing the LPS-induced activation of the reporter gene, we constructed an 0.8-kb Pai-2 reporter gene by deleting the sequence from −2.7 to −0.8 kb, which contained the previously reported NF-κB site (see Fig. S2 in the supplemental material). With this 0.8-kb Pai-2 construct, the addition of AhR and p65 no longer enhanced the activity in response to LPS treatment (Fig. 5A), indicating that the sequence between −0.8 and −2.7 kb, containing an NF-κB site, is responsible for enhancing Pai-2 gene activation in response to AhR and NF-κB. Further downstream, we noticed the presence of a putative C/EBPβ binding sequence (around 250 base pairs upstream of the transcription initiation site), which has been reported to be responsible for LPS-induced activation of the gene (4). Deletion or point mutation of this sequence was found to abrogate the ability of LPS to induce this gene, indicating that this C/EBPβ binding site functions as an enhancer sequence in the LPS response (see Fig. S2 in the supplemental material).

Recruitment of transcription factors necessary for LPS-induced Pai-2 expression. When macrophages were treated with LPS, p65 translocated from the cytoplasm into the nucleus independently of AhR (Fig. 5B), as reported previously. However, without AhR, ChIP revealed that p65 was not recruited to the enhancer sequence in the Pai-2 gene, which contains an NF-κB site (Fig. 5E). In WT macrophages, nuclear-translocated p65 was only recruited to the enhancer sequence of the Pai-2 gene together with AhR. PolII was concomitantly recruited to the TATA sequence of the Pai-2 gene in AhR WT but not AhR KO macrophages. Surprisingly, we observed that LPS induced AhR binding to the Pai-2 NF-κB site, as shown by ChIP using an anti-AhR antiserum. Co-IP assays revealed that AhR and p65 interacted in macrophages (Fig. 5C), consistent with a previous report (31). On the other hand, expression of the Cox-2 gene is known to be activated by LPS through recruitment of p65 to its NF-κB binding site, and this occurs independent of AhR (Fig. 5D), with concomitant binding of PolII to the transcription initiation site (TATA) of the Cox-2 gene (Fig. 5E). Arnt was not recruited to the Pai-2 promoter by ChIP assay (data not shown), consistent with normal Pai-2 expression in the macrophages from $Arnt^{flox/-}$::LysM Cre mice (Fig. 4D).

As shown in Fig. S3 in the supplemental material, the CCAAT box sequence in the Pai-2 gene was recognized by C/EBPβ in an LPS-dependent manner in both AhR WT and KO macrophages. This binding of C/EBPβ to the Pai-2 pro-

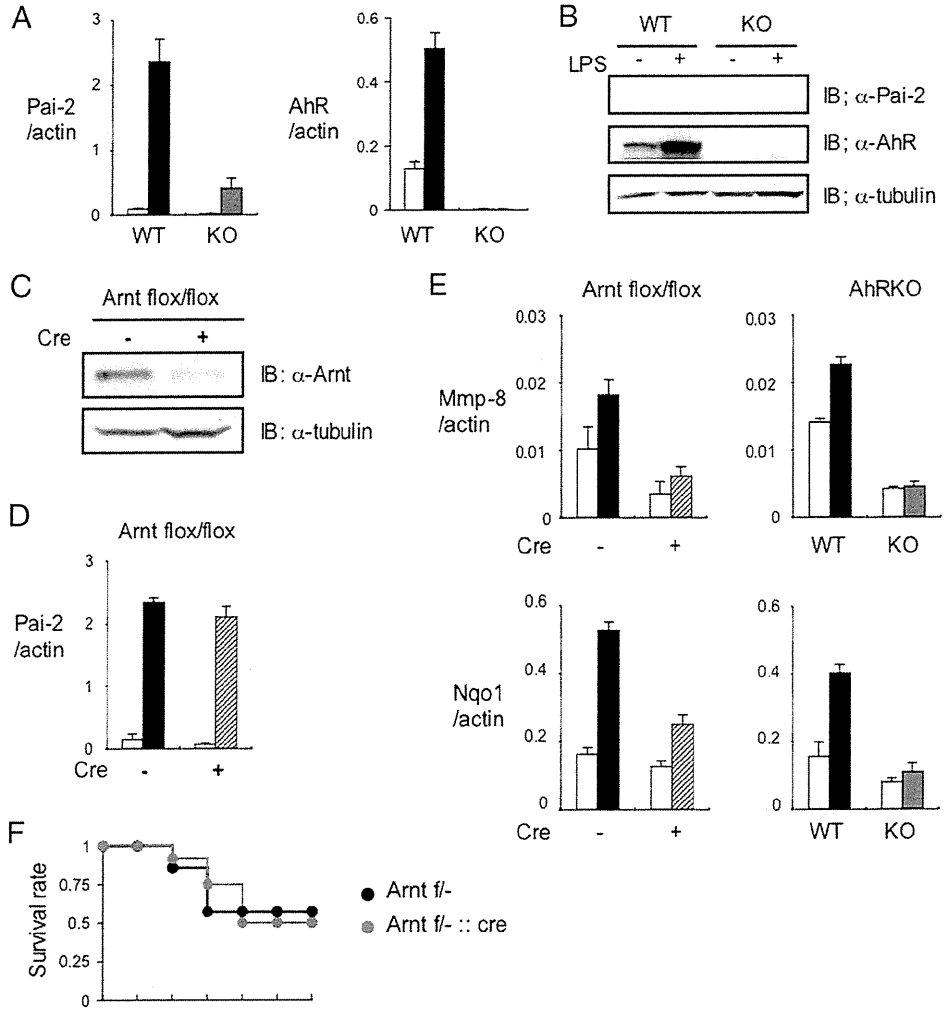

FIG. 4. Arnt is not required for LPS-induced enhancement of Pai-2 expression. (A) Relative Pai-2 and AhR mRNA expression levels in AhR WT and AhR KO PEMs 4 h after treatment with (black or gray bars) or without (white bars) LPS (10 ng/ml). (B) Immunoblot analysis of Pai-2 and AhR expression in AhR WT and KO PEMs after a 16-h incubation with LPS (10 ng/ml). (C) Immunoblot analysis of Arnt in $Arnt^{flox/flox}$ and $Arnt^{flox/flox}$::LysM Cre PEMs. (D) Relative Pai-2 mRNA expression levels 4 h after incubation of $Arnt^{flox/flox}$ (black bar) and $Arnt^{flox/flox}$::LysM Cre (hatched bar) PEMs with LPS (10 ng/ml). (E) Left, relative expression levels of Mmp-8 and Nqo1 mRNA in $Arnt^{flox/flox}$ (black bar) and $Arnt^{flox/flox}$::LysM Cre (hatched bar) PEMs treated with DMSO (white bars) or 3MC (black or hatched bar) (1 μM). Right, relative expression levels of Mmp-8 and Nqo1 mRNA in AhR WT (black bar) and AhR KO (gray bar) PEMs treated with DMSO (white bars) or 3MC (black or gray bar) (1 μM). (F) Survival of $Arnt^{flox/-}$ (Arnt f/−; n = 7) and $Arnt^{flox/-}$::LysM Cre (Arnt f/−::cre; n = 12) mice after LPS challenge (25 mg/ml). Error bars show standard deviations. IB, immunoblot; +, present; −, absent; α, anti.

moter might explain the weak LPS-induced activation of Pai-2 gene expression in AhR KO macrophages (Fig. 4A; also see Fig. S3 in the supplemental material), as described in the previous section.

The requirement of the functional domains of AhR for AhR-dependent Pai-2 expression. To determine the functional domains of AhR for AhR-dependent Pai-2 expression, we investigated the Pai-2 expression in ANA-1 cells, which were transfected with various AhR mutants (Fig. 6). Compared with the levels in ANA-1 cells transfected with full-length AhR, we observed much lower levels of expression of Pai-2 in the ANA-1 cells transfected with AhR NLSm (a mutant located predominantly in the cytoplasm) (Fig. 6B, bars 3, 4, 11, and 12). On the other hand, transfection with AhR CA (a constitutively active mutant located predominantly in the nucleus) gave a result for Pai-2 expression comparable to that of the transfection with full-length AhR (Fig. 6B, bars 3, 4, 7, and 8). These results indicated that nuclear AhR functions in AhR-dependent Pai-2 expression. The fractionation of AhR indicated that a small but significant amount of AhR existed in the nucleus without treatment with ligands such as 3MC, in contrast with the large amount in the cytoplasm (Fig. 5B), consistent with the previous report that AhR has functional nuclear localization signal and nuclear export signal sequences and shuttles between the cytoplasm and nucleus. It is reported that when nuclear export is inhibited by trichomycin B or phosphorylation at S68, AhR accumulates in the nucleus (12). Therefore, it could be considered that in macrophages, AhR is in-

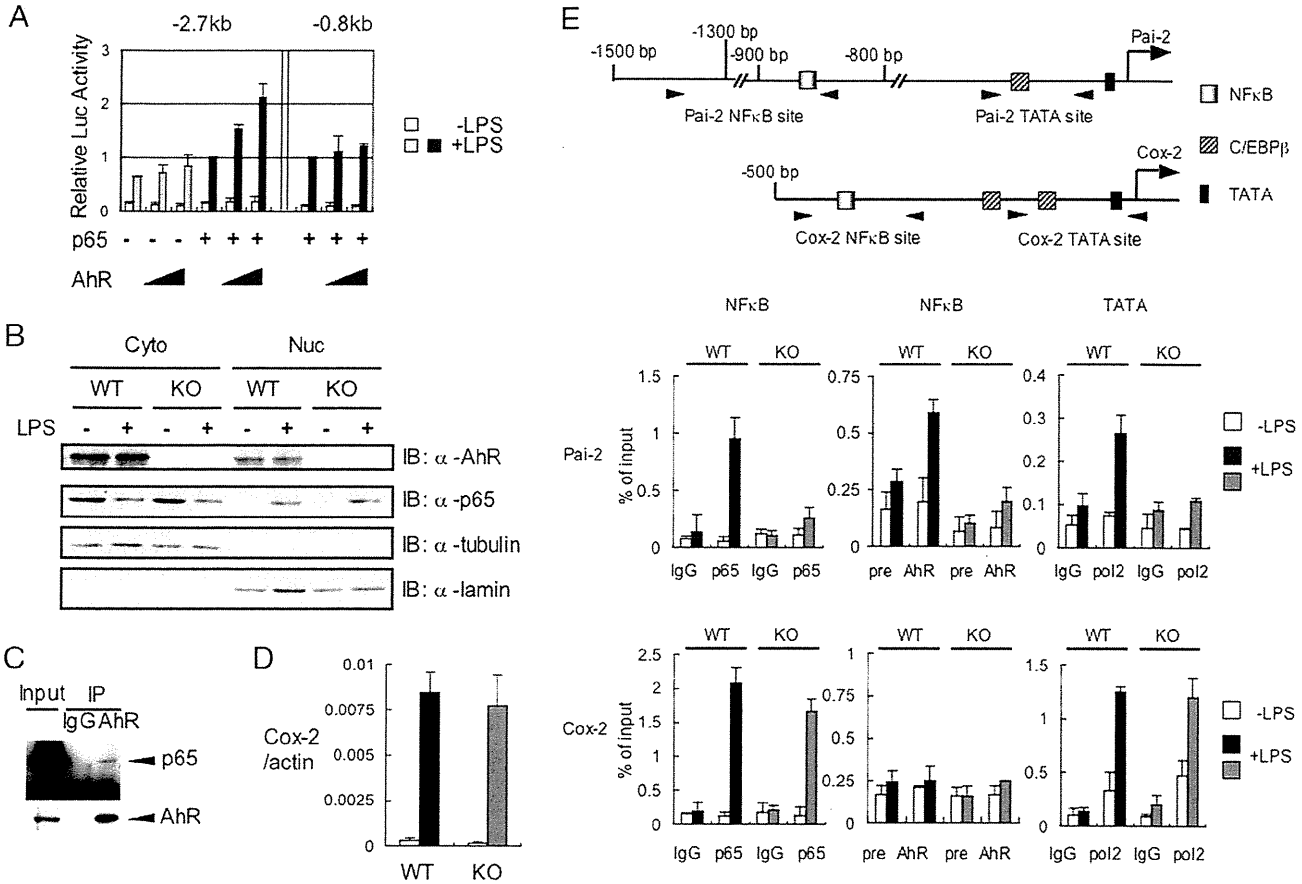

FIG. 5. Recruitment of transcription factors necessary for LPS-induced Pai-2 expression. (A) LPS-induced luciferase expression from the Pai-2 (−2.7 kb) and Pai-2 (−0.8 kb) reporter genes. RAW 264.7 cells were transfected with each reporter gene, with and without pcDNA3-AhR (0 ng, 50 ng, 100 ng) and/or pcDNA3-p65 (1 ng). Values represent the means, normalized to *Renilla* luciferase activity (used as an internal control), ± standard deviations of the results of three independent experiments. The activities shown by the fourth and seventh pairs of bars were used as standards for normalizing the relative activities of the other conditions. (B) AhR WT and AhR KO PEMs were left untreated or were treated with LPS for 1 h. Cytoplasmic (Cyto) and nuclear (Nuc) extracts were immunoblotted with antibodies against AhR, p65, tubulin, and lamin. (C) Co-IP of AhR and p65. Whole-cell extracts from AhR WT PEMs were coimmunoprecipitated with anti-AhR antibody. Co-IPs and Western blotting were performed as described in Materials and Methods. (D) Relative expression levels of Cox-2 mRNA in AhR WT and AhR KO PEMs after 4 h of treatment with or without LPS (10 ng/ml). Bars are as labeled in panel A. Error bars show standard deviations. (E) Top, transcription factor binding sites in the Pai-2 and Cox-2 genes. Bottom, results of ChIP analyses of the Pai-2 and Cox-2 promoters. ChIP analyses were performed using antibodies to p65, AhR, and PolII in LPS-induced AhR WT and AhR KO PEMs. ChIP analyses and real-time PCRs were performed as described in Materials and Methods. Error bars show standard deviations. +, present; −, absent; α, anti; IgG, immunoglobulin G.

volved in Pai-2 expression induced by LPS treatment in the absence of typical AhR ligands (Fig. 4A). The mechanism of AhR's involvement in Pai-2 expression induced by LPS will be investigated in detail. To further address the question of the requirement for the AhR domain in Pai-2 expression, we generated ANA-1 cells stably transfected with AhR ΔC (an activation domain-deficient mutant) and AhR Y9F (the mutant with attenuated DNA binding) (18). Compared with the expression in stable ANA-1 cells transfected with full-length AhR, neither of the cell lines transfected with AhR ΔC or AhR Y9F significantly expressed Pai-2 (Fig. 6B, bars 3 to 6, 9, and 10). These results indicate that both the activation and DNA binding domains of AhR were required for AhR-dependent Pai-2 expression. Co-IP analysis using these AhR mutants showed that the N-terminal region of AhR (AhR ΔC mutant) interacted with p65 (Fig. 6C).

DISCUSSION

AhR was originally found as a transcription factor that was involved in the induction of xenobiotic-metabolizing CYP1A1 by TCDD and other PAHs and has been found to act as a multifunctional regulatory factor in areas ranging from drug metabolism to innate immunity, providing protection against invading xenobiotics. Close investigation of the phenotypes of AhR KO mice revealed that they seem to suffer from morbidity from impaired immunity and easily succumb to bacterial infection. We examined the susceptibility of AhR KO mice to LPS-induced septic shock and found that they were hypersensitive to LPS treatment and had increased secretion of proinflammatory cytokines, such as IL-1β, TNF-α, IL-18, and IFN-γ (Fig. 1A and B). It has been reported that in endotoxic shock, IL-1β and TNF-α are rapidly released and trigger a secondary

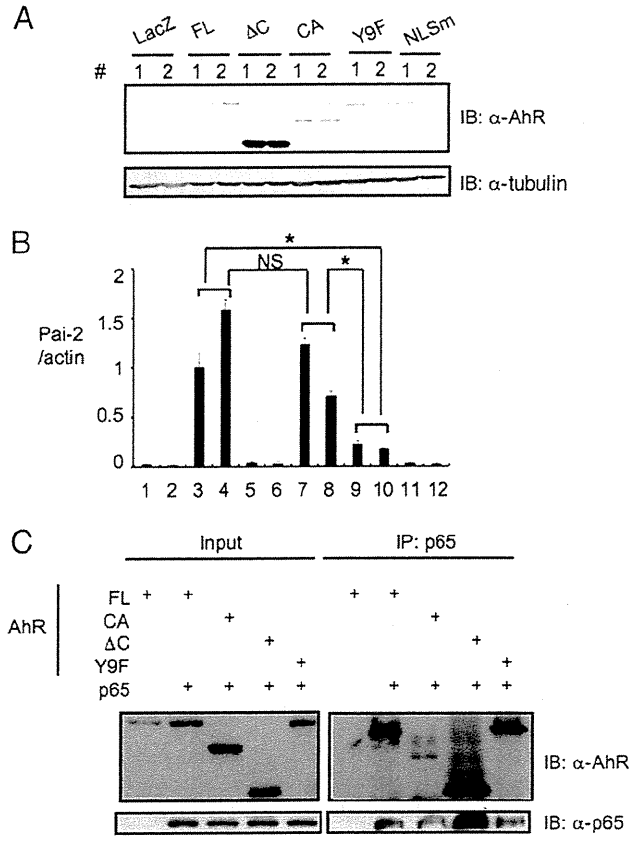

FIG. 6. Nuclear localization, activation, and DNA binding domains of AhR are required for AhR-dependent Pai-2 expression. (A) Immunoblot analysis of full-length AhR or mutants in LacZ or AhR transformant ANA-1 cells. Paired lanes labeled 1 and 2 show results from experiments using two independent transformants. (B) Relative expression levels of Pai-2 mRNA in ANA-1 cells transfected with LacZ or full-length AhR or mutants. Bars show quantification of the results in the 12 lanes in panel A; error bars show standard deviations. *, $P < 0.001$; NS, not significant. (C) Interaction of p65 and AhR mutants. Co-IP of p65 and full-length AhR or mutants expressed in 293T cells, using anti-p65 antibody. AhR FL (full-length) comprises amino acids 1 to 805, AhR ΔC comprises amino acids 1 to 544, and AhR CA comprises amino acids 1 to 276 and 419 to 805; in AhR Y9F, Y9 was mutated to F; and in AhR NLSm 37R, 38H, and 39R were mutated to A, G, and S, respectively. IB, immunoblot; α, anti; +, present.

inflammatory cascade that is dependent on the transcription factor NF-κB (10). Mice with a macrophage-specific conditional deletion of AhR ($AhR^{flox/-}$::LysM Cre) were more susceptible to LPS-induced septic shock than $AhR^{flox/-}$ mice, indicating that the dysfunction of macrophages due to AhR deficiency is one of the major causes of the enhanced susceptibility of AhR KO mice to LPS-induced septic shock (Fig. 2A). Consistent with these observations, isolated AhR KO BMDM secreted much larger amounts of IL-1β and had a slight increase in TNF-α in response to LPS (Fig. 2B). Since IL-1β mRNA levels were not altered between AhR KO and AhR WT BMDM (Fig. 2C), the increased IL-1β secretion is probably not due to the enhanced synthesis but, rather, is likely due to enhanced processing of IL-1β. (16).

We thought that this IL-1β oversecretion by AhR-deficient macrophages might provide clues as to how AhR functions as a physiological immunosuppressor. Microarray analyses to comprehensively investigate the AhR-dependent changes in gene expression that were responsible for increased IL-1β secretion revealed that the levels of expression of Pai-2 and Bcl-2 mRNA were markedly reduced in AhR KO BMDM, which was confirmed by real-time PCR (Fig. 3B). Reconstitution experiments with adenoviruses showed that only Pai-2 expression could significantly suppress IL-1β oversecretion in AhR KO macrophages, while no suppressive effect was observed with Bcl-2 expression (Fig. 3C). It has been reported that there are several pathways for processing IL-1β that lead to its secretion (16). These results indicate that Pai-2 and Bcl-2 are differentially involved in these pathways. Recently, in experiments using ΔIKKβ myeloid mice, Pai-2 has been reported to suppress IL-1β secretion, acting downstream of NF-κB (10). The IL-1β processing that is regulated by the inflammasome involves caspase-1 (16). Consistent with these observations, treatment with caspase inhibitors, Z-YVAD-FMK and Z-VAD-FMK markedly reduced the secretion of IL-1β in AhR KO BMDM (Fig. 3A). It has also been reported that IL-18 processing is regulated by the same mechanism as IL-1β, which is consistent with the marked increase in plasma IL-18 levels ($P < 0.001$) observed in LPS-injected AhR KO mice (Fig. 1B). Stimulation of the inflammasome involving caspase-1 usually requires secondary signals, such as high ATP concentrations. Interestingly, however, the IL-1β oversecretion resulting from AhR deficiency did not seem to require any other stimulation besides LPS, which is in accordance with the report on the IKKβ Δmyeloid mice (10). Further investigation will be required to address the molecular details of Pai-2-regulated IL-1β secretion.

Although it has been reported that Pai-2 mRNA was induced by a typical AhR ligand, TCDD (27), we did not find any obvious XRE sequences (GCGTG) in the 5-kb regions upstream or downstream of the transcription start site of the mouse Pai-2 promoter. However, these promoter regions rendered a reporter gene responsive to LPS (Fig. 5A and E). This sequence search suggested that AhR might not regulate Pai-2 gene expression in the canonical way (i.e., heterodimerized with Arnt) and led us to investigate whether Arnt was involved in LPS-induced Pai-2 regulation. In experiments with Arnt-deficient and Arnt siRNA-expressing macrophages, we demonstrated that AhR enhanced Pai-2 expression in an Arnt-independent manner (Fig. 4D; also see Fig. S1 in the supplemental material). Arnt2 is considered to be another possible alternative (11), but we have previously shown that AhR interacts predominantly with Arnt but not with Arnt2 (27). Therefore, it is highly likely that AhR enhances Pai-2 expression independently of Arnt family proteins (11). It was previously reported that LPS induced Pai-2 expression through activation of NF-κB (21) and that AhR physically interacted with p65 (31) to activate or inhibit gene expression in a context-dependent manner (31). In our reporter gene assay using RAW 264.7 cells, the Pai-2 reporter gene required both NF-κB and AhR for a high level of expression in response to LPS treatment (Fig. 5A). In AhR KO macrophages, LPS treatment induced nuclear translocation of p65 (Fig. 5B), but it was not recruited to the NF-κB-binding site of the Pai-2 gene, which confers LPS inducibility (Fig. 5E), suggesting that AhR is required for recruitment of p65 to this site, which may be a

crossing point between AhR and NF-κB signaling pathways. In WT macrophages, AhR and p65 were recruited to the same DNA sequence by the LPS treatment (Fig. 5E), and they interacted directly (Fig. 5C and 6C), leading to the recruitment of PolII to the TATA sequence of the transcription initiation site. In contrast, p65 was recruited to the Cox-2 promoter in response to LPS treatment in AhR KO macrophages. The detailed molecular basis for how p65 binds differentially to the Pai-2 and Cox-2 genes remains to be investigated.

It was also reported that AhR interacts with RelB on chemokine promoters, such as IL-8, in response to TCDD treatment, enhancing their expression (33). Although an AhR-RelB binding DNA sequence, designated RelBAhRE (GGGTGC AT), was found near the NF-κB site in the Pai-2 promoter, the expression of the Pai-2 (−2.7 kb) Luc reporter gene was not enhanced by RelB and AhR coexpression (data not shown), suggesting that RelB may not function as a partner for AhR in inducing Pai-2 expression. Since the AhR DNA binding activity was suggested by the results of the experiment using the AhR Y9F mutant to be required for AhR-dependent Pai-2 expression (Fig. 6B, bars 3, 4, 9, and 10), the possibility could be raised that an AhR and p65 heterodimer might work as a transcription factor by binding the RelBAhRE sequence. However, the experiments using the reporter gene containing a tandem arrangement of four RelBAhRE sequences did not showed enhanced expression of the reporter gene expression with coexpression of AhR and p65. It remains to be investigated in detail how AhR and p65 activate the Pai-2 promoter. AhR has been reported to have the nuclear localization signal and nuclear export signal sequences and to shuttle between nucleus and cytoplasm. Inhibition of nuclear export of AhR by trichomycin B or phosphorylation reportedly leads to the accumulation of AhR in the nucleus (12). Consistent with these findings, a small part of AhR was observed in the nuclei of macrophages under normal conditions. Upon treatment with LPS, nuclear AhR should accumulate due to phosphorylation downstream of the LPS signaling pathway or p65, reported to be translocated into the nucleus (21), should be recruited to the Pai-2 promoter with the nuclear AhR.

Recently, there have been growing lines of evidence that AhR plays a crucial role in differentiation of the Th cell subsets Th1, Treg, and Th17 from naive CD4 T cells. It was reported that differentiation of these regulatory T cells from AhR KO naive T cells was significantly impaired under their respective polarizing conditions. AhR is reported to be highly induced under these conditions (14, 20, 23, 32), and AhR ligands further stimulated the tendency to their respective differentiations by molecular mechanisms that are largely unknown. In macrophages, AhR was also induced by LPS treatment (Fig. 4A and B) and negatively regulated the secretion of certain inflammatory cytokines, such as IL-1β and IL-18, most likely through the expression of Pai-2. Since AhR is a ligand-activated transcription factor and is known to be ubiquitously expressed in immune cells (13), this raises the possibility that an appropriate AhR ligand may be useful for treating patients with inflammatory disorders.

ACKNOWLEDGMENTS

We thank L. Varesio for kindly providing ANA-1 cells and Y. Watanabe and S. Ooba for mouse maintenance. We also thank Y. Nemoto for clerical work.

This work was funded in part by Solution Oriented Research for Science and Technology from Japan Science and Technology, Japan Science and Technology Agency, Kawaguchi, Japan, and by a grant for Scientific Research from the Ministry of Health, Labor and Welfare, Japan.

REFERENCES

1. **Abbott, B., J. Schmid, J. Pitt, A. Buckalew, C. Wood, G. Held, and J. Diliberto.** 1999. Adverse reproductive outcomes in the transgenic Ah receptor-deficient mouse. Toxicol. Appl. Pharmacol. **155**:62–70.
2. **Baba, T., J. Mimura, N. Nakamura, N. Harada, M. Yamamoto, K. Morohashi, and Y. Fujii-Kuriyama.** 2005. Intrinsic function of the aryl hydrocarbon (dioxin) receptor as a key factor in female reproduction. Mol. Cell. Biol. **25**:10040–10051.
3. **Blasi, E., D. Radzioch, S. Durum, and L. Varesio.** 1987. A murine macrophage cell line, immortalized by v-raf and v-myc oncogenes, exhibits normal macrophage functions. Eur. J. Immunol. **17**:1491–1498.
4. **Bradley, M., L. Zhou, and S. Smale.** 2003. C/EBPbeta regulation in lipopolysaccharide-stimulated macrophages. Mol. Cell. Biol. **23**:4841–4858.
5. **Bruey, J., N. Bruey-Sedano, F. Luciano, D. Zhai, R. Balpai, C. Xu, C. Kress, B. Bailly-Maitre, X. Li, A. Osterman, S. Matsuzawa, A. Terskikh, B. Faustin, and J. Reed.** 2007. Bcl-2 and Bcl-XL regulate proinflammatory caspase-1 activation by interaction with NALP1. Cell **129**:45–56.
6. **Fernandez-Salguero, P., D. Hilbert, S. Rudikoff, J. Ward, and F. Gonzalez.** 1996. Aryl-hydrocarbon receptor-deficient mice are resistant to 2,3,7,8-tetrachlorodibenzo-p-dioxin-induced toxicity. Toxicol. Appl. Pharmacol. **140**: 173–179.
7. **Fernandez-Salguero, P., T. Pineau, D. Hilbert, T. McPhail, S. Lee, S. Kimura, D. Nebert, S. Rudikoff, J. Ward, and F. Gonzalez.** 1995. Immune system impairment and hepatic fibrosis in mice lacking the dioxin-binding Ah receptor. Science **268**:722–726.
8. **Fernandez-Salguero, P., J. Ward, J. Sundberg, and F. Gonzalez.** 1997. Lesions of aryl-hydrocarbon receptor-deficient mice. Vet. Pathol. **34**:605–614.
9. **Fujii-Kuriyama, Y., and J. Mimura.** 2005. Molecular mechanisms of AhR functions in the regulation of cytochrome P450 genes. Biochem. Biophys. Res. Commun. **338**:311–317.
10. **Greten, F., M. Arkan, J. Bollrath, L. Hsu, J. Goode, C. Miething, S. Göktuna, M. Neuenhahn, J. Fierer, S. Paxian, N. Van Rooijen, Y. Xu, T. O'Cain, B. Jaffee, D. Busch, J. Duyster, R. Schmid, L. Eckmann, and M. Karin.** 2007. NF-kappaB is a negative regulator of IL-1beta secretion as revealed by genetic and pharmacological inhibition of IKKbeta. Cell **130**:918–931.
11. **Hirose, K., M. Morita, M. Ema, J. Mimura, H. Hamada, H. Fujii, Y. Saijo, O. Gotoh, K. Sogawa, and Y. Fujii-Kuriyama.** 1996. cDNA cloning and tissue-specific expression of a novel basic helix-loop-helix/PAS factor (Arnt2) with close sequence similarity to the aryl hydrocarbon receptor nuclear translocator (Arnt). Mol. Cell. Biol. **16**:1706–1713.
12. **Ikuta, T., Y. Kobayashi, and K. Kawajiri.** 2004. Cell density regulates intracellular localization of aryl hydrocarbon receptor. J. Biol. Chem. **279**:19209–19216.
13. **Kerkvliet, N.** 2009. AHR-mediated immunomodulation: the role of altered gene transcription. Biochem. Pharmacol. **77**:746–760.
14. **Kimura, A., T. Naka, K. Nohara, Y. Fujii-Kuriyama, and T. Kishimoto.** 2008. Aryl hydrocarbon receptor regulates Stat1 activation and participates in the development of Th17 cells. Proc. Natl. Acad. Sci. USA **105**:9721–9726.
15. **Lund, A., M. Goens, B. Nuñez, and M. Walker.** 2006. Characterizing the role of endothelin-1 in the progression of cardiac hypertrophy in aryl hydrocarbon receptor (AhR) null mice. Toxicol. Appl. Pharmacol. **212**:127–135.
16. **Martinon, F., and J. Tschopp.** 2007. Inflammatory caspases and inflammasomes: master switches of inflammation. Cell Death Differ. **14**:10–22.
17. **Mimura, J., K. Yamashita, K. Nakamura, M. Morita, T. Takagi, K. Nakao, M. Ema, K. Sogawa, M. Yasuda, M. Katsuki, and Y. Fujii-Kuriyama.** 1997. Loss of teratogenic response to 2,3,7,8-tetrachlorodibenzo-p-dioxin (TCDD) in mice lacking the Ah (dioxin) receptor. Genes Cells **2**:645–654.
18. **Minsavage, G. D., S. Park, and T. A. Gasiewicz.** 2004. The aryl hydrocarbon receptor (AhR) tyrosine 9, a residue that is essential for AhR DNA binding activity, is not a phosphoresidue but augments AhR phosphorylation. J. Biol. Chem. **279**:20582–20593.
19. **Muruve, D., V. Pétrilli, A. Zaiss, L. White, S. Clark, P. Ross, R. Parks, and J. Tschopp.** 2008. The inflammasome recognizes cytosolic microbial and host DNA and triggers an innate immune response. Nature **452**:103–107.
20. **Negishi, T., Y. Kato, O. Ooneda, J. Mimura, T. Takada, H. Mochizuki, M. Yamamoto, Y. Fujii-Kuriyama, and S. Furusako.** 2005. Effects of aryl hydrocarbon receptor signaling on the modulation of TH1/TH2 balance. J. Immunol. **175**:7348–7356.
21. **Park, J., F. Greten, A. Wong, R. Westrick, J. Arthur, K. Otsu, A. Hoffmann, M. Montminy, and M. Karin.** 2005. Signaling pathways and genes that inhibit pathogen-induced macrophage apoptosis—CREB and NF-kappaB as key regulators. Immunity **23**:319–329.
22. **Petrulis, J., and G. Perdew.** 2002. The role of chaperone proteins in the aryl hydrocarbon receptor core complex. Chem. Biol. Interact. **141**:25–40.

23. **Quintana, F., A. Basso, A. Iglesias, T. Korn, M. Farez, E. Bettelli, M. Caccamo, M. Oukka, and H. Weiner.** 2008. Control of T(reg) and T(H)17 cell differentiation by the aryl hydrocarbon receptor. Nature **453**:65–71.
24. **Schmidt, J., G. Su, J. Reddy, M. Simon, and C. Bradfield.** 1996. Characterization of a murine Ahr null allele: involvement of the Ah receptor in hepatic growth and development. Proc. Natl. Acad. Sci. USA **93**:6731–6736.
25. **Schreiber, E., P. Matthias, M. Müller, and W. Schaffner.** 1989. Rapid detection of octamer binding proteins with 'mini-extracts,' prepared from a small number of cells. Nucleic Acids Res. **17**:6419.
26. **Schwartz, B., and J. Bradshaw.** 1992. Regulation of plasminogen activator inhibitor mRNA levels in lipopolysaccharide-stimulated human monocytes. Correlation with production of the protein. J. Biol. Chem. **267**:7089–7094.
27. **Sekine, H., J. Mimura, M. Yamamoto, and Y. Fujii-Kuriyama.** 2006. Unique and overlapping transcriptional roles of arylhydrocarbon receptor nuclear translocator (Arnt) and Arnt2 in xenobiotic and hypoxic responses. J. Biol. Chem. **281**:37507–37516.
28. **Sogawa, K., R. Nakano, A. Kobayashi, Y. Kikuchi, N. Ohe, N. Matsushita, and Y. Fujii-Kuriyama.** 1995. Possible function of Ah receptor nuclear translocator (Arnt) homodimer in transcriptional regulation. Proc. Natl. Acad. Sci. USA **92**:1936–1940.
29. Reference deleted.
30. **Takagi, S., H. Tojo, S. Tomita, S. Sano, S. Itami, M. Hara, S. Inoue, K. Horie, G. Kondoh, K. Hosokawa, F. Gonzalez, and J. Takeda.** 2003. Alteration of the 4-sphingenine scaffolds of ceramides in keratinocyte-specific Arnt-deficient mice affects skin barrier function. J. Clin. Investig. **112**:1372–1382.
31. **Tian, Y., S. Ke, M. Denison, A. Rabson, and M. Gallo.** 1999. Ah receptor and NF-kappaB interactions, a potential mechanism for dioxin toxicity. J. Biol. Chem. **274**:510–515.
32. **Veldhoen, M., K. Hirota, A. Westendorf, J. Buer, L. Dumoutier, J. Renauld, and B. Stockinger.** 2008. The aryl hydrocarbon receptor links TH17-cell-mediated autoimmunity to environmental toxins. Nature **453**:106–109.
33. **Vogel, C., E. Sciullo, W. Li, P. Wong, G. Lazennec, and F. Matsumura.** 2007. RelB, a new partner of aryl hydrocarbon receptor-mediated transcription. Mol. Endocrinol. **21**:2941–2955.

The Journal of Toxicological Sciences (J. Toxicol. Sci.)
Vol.34, Special Issue II, SP279-SP286, 2009

Intrauterine environment-genome interaction and Children's development (2): Brain structure impairment and behavioral disturbance induced in male mice offspring by a single intraperitoneal administration of domoic acid (DA) to their dams

Kentaro Tanemura, Katsuhide Igarashi, Toshiko-R Matsugami, Ken-ichi Aisaki, Satoshi Kitajima and Jun Kanno

Division of Cellular & Molecular Toxicology, Biological Safety Research Center, National Institute of Health Sciences, 1-18-1 Kamiyoga, Setagaya-ku, Tokyo 158-8501, Japan

(Received February 17, 2009)

ABSTRACT — To demonstrate induction of delayed central nervous toxicity by disturbing neuronal activities in the developing brain, we administered a single intraperitoneal dose of domoic acid (DA; 1 mg/kg), a potent glutamate receptor agonist, to pregnant female mice at the gestational day of 11.5, 14.5 or 17.5. The dams had recovered from acute symptoms within 24 hr, followed by normal delivery, feeding and weaning. All male offspring mice after weaning were apparently normal in response to handlers during cage maintenance, body weight measurement and to mate mice in group housing conditions. At the age of 11 weeks, our neurobehavior testing battery revealed severe impairment of learning and memory with serious deviances of anxiety-related behaviors. The developed brain of prenatally exposed mice showed myelination failure and the overgrowth of neuronal processes of the limbic cortex neurons. This study indicates that the temporal disturbance of neurotransmission of the developing brain induces irreversible structural and functional damage to offspring which becomes monitorable in their adulthood by a proper battery of neurobehavioral tests.

Key words: Domoic acid, Prenatal exposure, Brain structure, Behavior

INTRODUCTION

Adequate neural activities are necessary for the maturation of neural networks during brain development (Rice and Barone, 2000). Historically, the presence of such plasticity-driven mechanisms has been demonstrated by a series of studies of eyelid suture in kittens or monkeys and corresponding findings reported in young human cataracta patients (Wiesel, 1982; Gu *et al.*, 1989; Fonta *et al.*, 2000). These processes require proper stimuli to the brain that trigger the release of neurotransmitters from the neurons and subsequent receptor-mediated signal transduction (Ooi and Wood, 2008; Greer and Greenberg, 2008; Cohen-Cory, 2002). Therefore, it is highly conceivable that disturbance of neural activities by neuroactive xenobiotics leads to malformation of the fine structure of the brain. Even when the exposure was transient, it would result in anomaly of higher brain functions in adulthood without overt signs of brain damage during maturation.

Glutamate receptors begin to express in the late embryonic stages, and their expression increases with the advance of brain development (Luján *et al.*, 2005; Manent *et al.*, 2005). Prenatal exposure of xenobiotic chemicals that interfere with the glutamate receptor function could induce malformation of the fine structure of the brain which should lead to anomaly of higher brain function that is different from acute neurotoxicity known for such chemicals to induce in adults (Bondy and Campbell, 2005). A marine biotoxin domoic acid (DA) which is structurally related to glutamate, and activates ionotropic α-amino-3-hydroxy-5-methyl-4-isoxazolepropionic acid (AMPA) and kinate subtypes of glutamate receptors (Pulido, 2008) is known to cause acute symptoms of diarrhea, seizures and memory loss in adult human by eating contaminated shellfish (Tryphonas and Iverson, 1990), and DA induced acute neurotoxicity in animal

Correspondence: Jun Kanno (E-mail: kanno@nihs.go.jp)

model (Chandrasekaran *et al.*, 2004). Additionally, DA is also known to cross the placenta, and enters prenatal brain tissue in rats (Maucher and Ramsdell, 2007). Therefore, prenatal exposure of DA may disrupt the neural activities by excessive stimulation of glutamate receptors, and should induce fine structural and functional disorganization in the developing brain. Here, we report that a transient transplacental DA exposure *in utero* induced alteration of the neurobehavioral parameters and corresponding fine brain structure of the male C57BL/6 mice in their adulthood.

MATERIALS AND METHODS

Animal treatment

All experiments were carried out under approval of Experimental Animal Use Committee of National Institute of Health Sciences, Japan. Pregnant C57LB/6 female mice obtained from Japan SLC, Inc., were individually housed in plastic breeding cages with free access to water and pellet diet (CRF-1; Oriental Yeast Co., Tokyo, Japan) in a 12 hr light-dark cycle conventional condition. Four groups with five pregnant mice each were prepared. All groups received three intraperitoneal injections on gestational day 11.5 (E11.5) as a late embryonic period, 14.5 (E14.5) and 17.5 (E17.5) as early and late fetal period respectively. Group A (Control) received three i.p. shots of saline on E11.5, E14.5 and E17.5. Group B (DA@E11.5) received one shot of DA (Calbiochem, San Diego, CA, USA) at a dosage of 1 mg/kg on E 11.5 and two shots of saline on E14.5 and E17.5. Group C (DA@14.5) received a shot of saline on E11.5, a shot of DA on E14.5 and another saline on E17.5. Group D (DA@E17.5) received two shots of saline on E11.5 and E14.5 , and a shot of DA on E17.5. The pups were weaned at 4 weeks of age, and four male mice per liter were randomly selected and housed in one cage with free access to water and CRF-1 pellet until 11 weeks of age.

Immunohistochemical analysis

Brains (n = 4 male mice per group) were fixed with methacarn fixative (methanol: chloroform:acetic acid, 60:30:10 v/v) and paraffin-embedded sections were prepared. Mouse monoclonal anti-microtubule associated protein 2 (MAP2, sc-32791; Santa Cruz, CA, USA), mouse monoclonal anti-neurofilament-m (NF-M, sc-20013; Santa Cruz, CA, USA), rabbit polyclonal anti-myelin associated glycoprotein (MAG, sc-15324; Santa Cruz, CA, USA), and rabbit polyclonal anti MAP2 (sc-20172; Santa Cruz, CA, USA) were used. Deparaffinized sections were pretreated with HistoVT-One (Nacalai Tesque, Kyoto, Japan.) as previously described (Tanemura *et al.*, 2005) and incubated with primary antibodies. Secondary antibodies were Alexa 568-conjugated anti-mouse IgG and Alexa 488-conjugated anti-rabbit IgG (Molecular Probes, Eugene, OR, USA). Fluorescent images were obtained with an FV-300 confocal laser scanning microscope (Olympus, Tokyo, Japan). For semi-quantitative analysis of images, we calculated the ratio of fluorescence intensity compared to control mice (group A), by using the IMAGE J program (http://rsb.info.nih.gov/ij/index.html. National Institute of Health, Bethesda), after adjusting background noise (n = 4 images per mouse).

Neurobehavioral tests

A battery of neurobehavioral tests were conducted on open field test (OF), light/dark transition test (LD), elevated plus maze test (EP) and contextual/cued fear conditioning test (FZ). Experimental apparatuses and image analyzing softwares were obtained from O'Hara & Co., Ltd., Japan. Image analyzing softwares (Image OF4, Image LD2, Image EP2 and Image FZ2) were developed from the public domain IMAGE J program. All experiments were done with 8 mice per group (32 mice total), and were conducted between 13:30 and 16:30. The level of background noise during behavioural testing was about 50 dBA. After each trial, the apparatuses were wiped and cleaned.

Open field test

The locomotor activity was measured for 10 min using an open field apparatus made of white plastic (50 x 50 x 40 (H) cm).

An LED light system was positioned 50 cm above the centre of the field (50 lux at the centre of field). Total distance travelled (cm), time spent in the central area (30% of the field) (sec), and the frequencies of movement were measured (Tanemura *et al.*, 2002).

Light/dark transition test

The apparatus used for the light/dark transition test consisted of a cage (21 x 42 x 25(H) cm) divided into two chambers by a partition with an opening. One chamber is brightly illuminated (250 lux), whereas the other chamber is dark (2 lux). A mouse is placed into the dark area and allowed to move freely between the two chambers through the opening for 5 min. The latency for the first move to the light area, the total number of transitions and the time spent on each side were measured.

Elevated plus maze test

The plus-shaped apparatus consisted of four arms (25

x 5 cm) connected to a central square area (5 x 5 cm). Opposite two arms are enclosed with 20 cm-high transparent walls and other two are left open. The floor of the maze is made of white plastic plate and is elevated 60 cm above the room floor (200 lux at the centre of the apparatus). A mouse is placed to the central square area of the maze, facing one of the open arms, and the behavior was recorded for 10 min: total distance traveled (cm), total time on open arms and central square area (sec) and the total number of entry to any of the arms (Tanemura *et al.*, 2002).

Contextual/cued fear conditioning test

The apparatus consists of a conditioning chamber (or a test chamber) (17 x 10 x 10 (H) cm) made of clear plastic with ceiling and placed in a sound proof box. The chamber floor has stainless steel rods (2-mm diameter) spaced 5 mm apart for giving electric foot shock (0.1 mA, 3 sec duration) to the mouse. The soundproof box consists of white-coloured wood, and is equipped with an audio speaker and light source (35 lux at the centre of the floor). A CCD camera is positioned 20 cm above the ceiling of the chamber. During the conditioning trial (Day 1), mice are placed individually into the conditioning chamber in the sound proof box and, after 90 sec, they are given three tone-shock pairings (30 sec of tone, 75 dB, 10 KHz followed by 3 sec of electric shock at the end of tone, 0.1 mA) separated by 90 sec. Then they are returned to their home cage. Next day (Day 2), as a "contextual fear test", they are returned to the conditioning chamber without tone and shock for a 6-min. On the third day (Day 3), they are brought to a novel chamber of different make without stainless steel rods place in the sound proof box and, after a period of 3 min, only the conditioning tone is presented for 3 min (no shock was presented, 35 lux at the centre of the floor). The freezing response of mice was defined as a consecutive 2 sec period of immobility. Freezing rate (%) was calculated as [time freezing/session time] x 100 (Tatebayashi *et al.*, 2002).

Statistical analysis

Data were indicated as means ± S.D. Statistical analysis was conducted with student's t-test by using StatView (SAS Institute, Cary, NC, USA). A p-value of < 0.05 compared to the results of control male mice (group A) was considered statistically significant.

RESULTS

Effects on morphology of brain by prenatal exposure to DA

Offspring mice of all groups after weaning up to the age of 11 weeks were apparently normal in response to handlers during cage maintenance, body weight measurement and to mate mice in group housing conditions. Routine histological observation of the brain at 11 weeks old by hematoxylin-eosin staining could not reveal difference among the groups (data not shown). By immunohistochemical study on the same brain sections, reduced immuno-reactivity against the MAG, the marker for myelin, was detected in the cortices of group B (DA@11.5) and C (DA@14.5) compared to control (Figs. 1A-D and I). In contrast, increased immuno-reactivity against MAP2, the marker for neuronal dendrite, was indicated in the same area of group B (DA@11.5), C (DA@14.5) and D (DA@17.5) compared to control (Figs. 1E-H and J). Increased immuno-reactivity against MAP2 was also found in lateral area of CA3 hippocampus of group B (DA@11.5), C (DA@14.5) and D (DA@17.5) compared to control, whereas immuno-reactivity for MAP2 showed no significant difference in medial area of CA3 hippocampus among the groups (Figs. 2A-D and I). Immuno-reactivity against NF-M; the marker for neuronal axon, also showed no significant difference in the same area among the groups (Figs. 2E-H and J).

Effects on behavior by prenatal exposure of DA

In the OF test, the distance traveled was not different among the groups (Fig. 3A), the time spent in center area was significantly prolonged in group D (DA@17.5) mice (Fig. 3B). In the LD test, group C (DA@14.5) mice stayed in light area for longer time (Fig. 4A), and latency for the first move to light area was significantly shorter in group C (DA@14.5) and D (DA@17.5) (Fig. 4B). In the EP test, significantly increased distance traveled and time spent in the open area were detected for group B (DA@11.5), C (DA@14.5) and D (DA@17.5) (Figs. 5A and B). In the FZ test, both Day 1 and Day 2 freezing responses of group C (DA@14.5) and D (DA@17.5) were significantly reduced compared to control (Figs. 6A and B).

DISCUSSION

The expression levels of glutamate receptors starts to elevate at the fetal period, i.e. approximately from E14 (Luján *et al.*, 2005; Manent *et al.*, 2005). Exogenous glutamatergic stimuli at this period would affect the for-

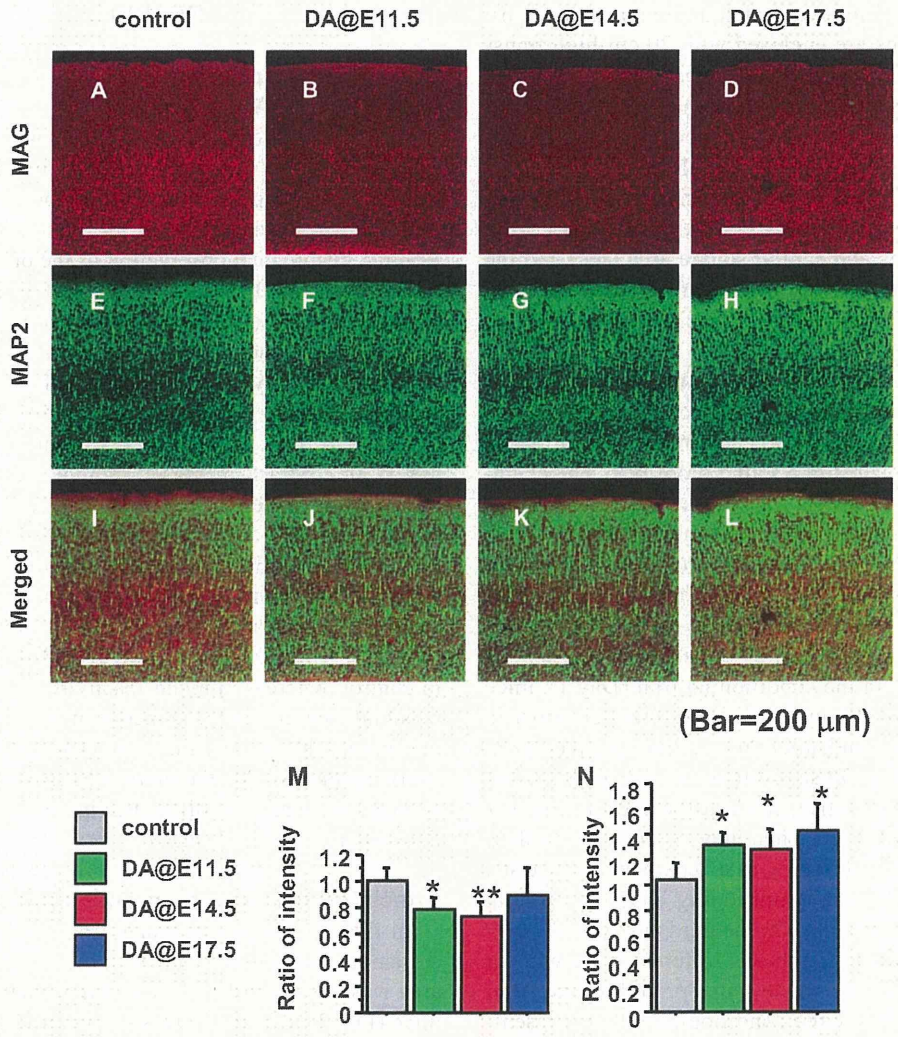

Fig. 1. Delayed effects on cerebral cortex induced by prenatal exposure of DA.
A-D, Immunohistochemical staining against MAG; E-H, immunohistochamical staining against MAP2; I-L, merged images of the cerebral cortex. A, E, I, group A (control), B, F, J, group B (DA@11.5), C, G, K, group C (DA@14.5) and D, H, L, group D (DA@17.5). Scale bar = 200 mm. M, Quantitative analysis in intensity ratio to control of MAG expression, and J, MAP2 expression among the groups (mean ± S.E.M.). Asterisk (**) and (*) indicate significant difference compared to control ($P < 0.01$) and ($P < 0.05$).

mation of the neural circuits. An extreme example to support this hypothesis would be the phenotype of the double knockout mouse of glutamate transportors GLT1 and GLAST (Matsugami *et al.*, 2006). Lack of these transportors is considered to result in abnormally high concentration of glutamate in the brain. In fact, morphological anomaly became apparent in synchronization with the expression of glutamine receptors. In our study, corresponding to the hypothesis, the neurobehavioral symptoms as a whole was severer for those exposed at fetal periods, i.e. E14.5 and E17.5, compared to those at embryonic period, i.e. E11.5 (Fig. 7).

We demonstrated that a prenatal exposure of a relatively low dose of DA induced a spectrum of neurobehavioral anomalies which became monitorable at the adult stage accompanied by alteration in fine brain structures detectable by immunohistochemistry. It is emphasized that this amount of DA did not induce abnormal responses dur-

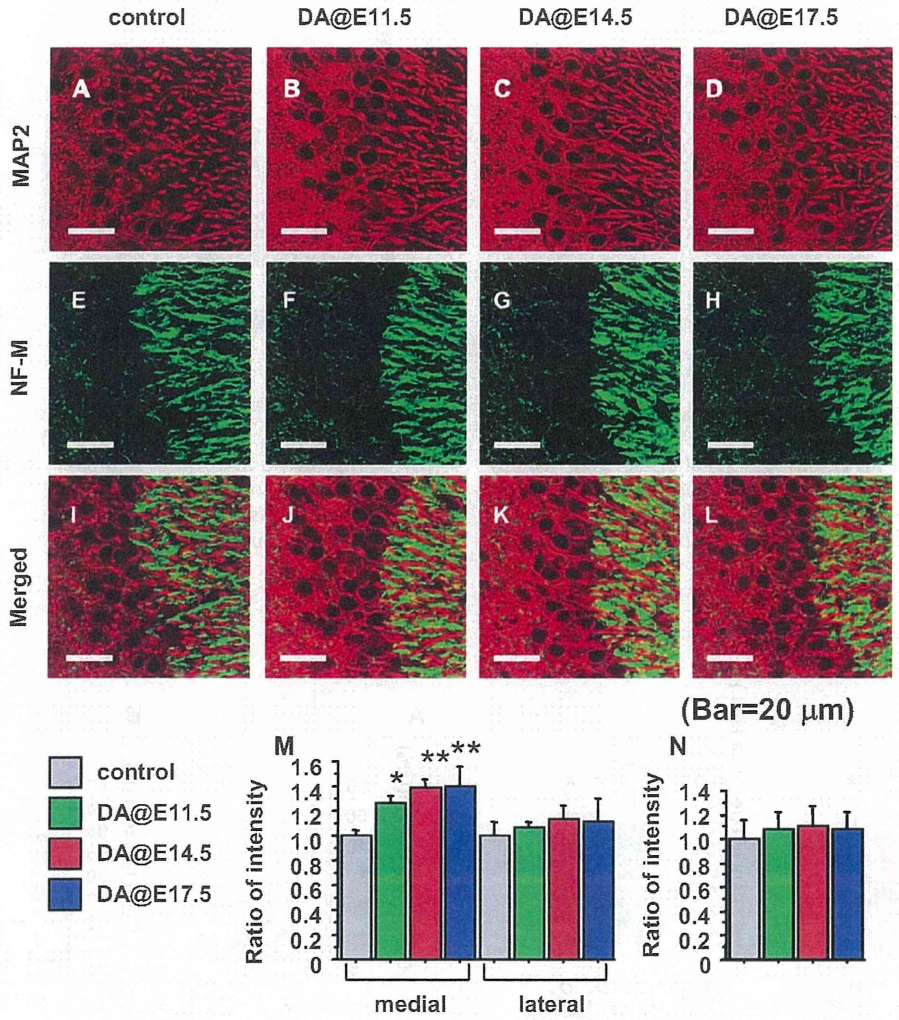

Fig. 2. Delayed effects on hippocampus induced by prenatal exposure of DA.
A-D, Immunohistochemical staining against MAP2; E-H, immunohistochamical staining against NF-M; I-L, merged images, of CA3 hippocampus. A, E, I, group A (control), B, F, J, group B (DA@11.5), C, G, K, group C (DA@14.5) and D, H, L, group D (DA@17.5). Scale bar = 200 mm. M, Quantitative analysis of MAP2 expression, and N, NF-M expression among the groups (mean ± S.E.M.). Asterisk (**) and (*) indicated significant difference compared to control ($P < 0.01$) and ($P < 0.05$).

ing maturation, such as hyperreactivity to handling and to cage mates, and did not present overt malformation of the brain detectable by the routine H&E histology at the age of 2 weeks (data not shown). It is also noted that the spectrum of the neurobehavioral symptoms induced in mice exposed to DA at adulthood was different from those monitored in this study (data not shown).

Although progressive hippocampal neuronal damages were reported to be induced by prenatal administration of DA (0.6 mg/kg intravenous injection to the dam) (Dakshinamurti *et al.*, 1993), we did not find notable neuronal loss or neuronal cell death as the delayed effects in adult mouse brain by prenatal exposure. On the other hand, we found myelination failure (Miller and Mi, 2007) in cortex of group B (DA@11.5) and C (DA@14.5) mice. And we also detected a finding compatible with the overgrowth of neuronal processes in cortex and hippocampus of group B (DA@11.5), C (DA@14.5) and D (DA@14.5)

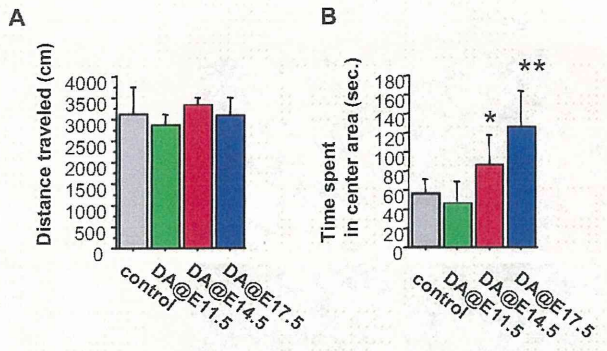

Fig. 3. Delayed effects on locomotor activity (OF test) induced by prenatal exposure of DA.
A, Mean distance travelled (total distances divided by total duration of trial, 10 min) and B, mean time spent in center area (30% of the field) in the open field apparatus (mean ± S.E.M.). Asterisk (**) and (*) indicated significant difference compared to control ($P < 0.01$) and ($P < 0.05$).

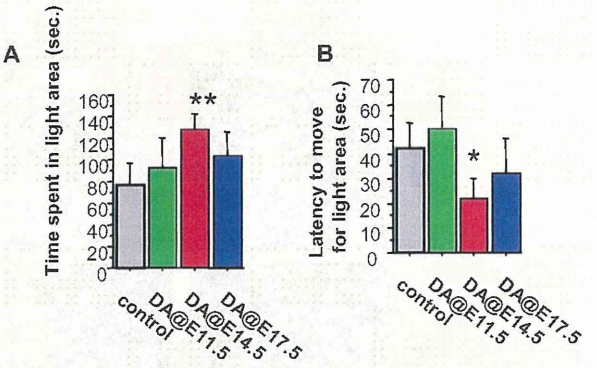

Fig. 4. Delayed effects on anxiety-related behavior (LD test) induced by prenatal exposure of DA.
A, Total time spent in light area, and B, latency time to move to light area in the LD apparatus (mean ± S.E.M.). Asterisk (**) and (*) indicated significant difference compared to control ($P < 0.01$) and ($P < 0.05$).

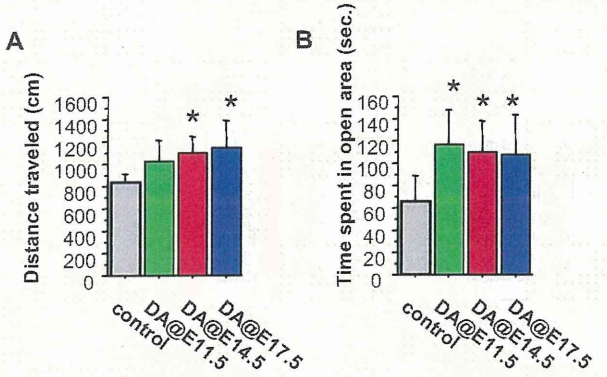

Fig. 5. Delayed effects on anxiety-related behavior (EP test) induced by prenatal exposure of DA.
A, Total distance travelled, and B, total time spent in open area in the elevated plus maze apparatus (mean ± S.E.M.). Asterisk (*) indicated significant difference compared to control ($P < 0.05$).

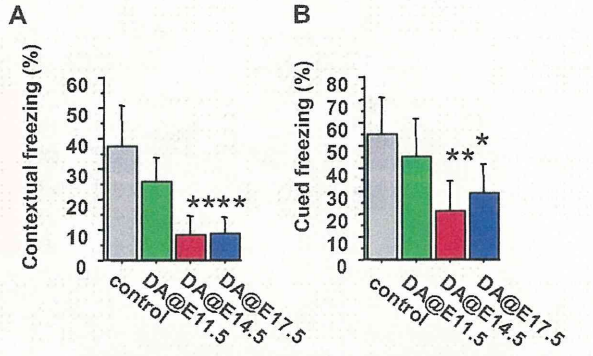

Fig. 6. Delayed effects on learning and memory (FZ test) induced by prenatal exposure of DA.
A, Contextual fear test and B, cued fear test. Memory performance is expressed as a mean percent duration of freezing responses (mean ± S.E.M.). Asterisk (**) and (*) indicated significant difference compared to control ($P < 0.01$) and ($P < 0.05$).

mice by using cytoskeletal marker. These findings indicated that the disorganization of brain was induced by the prenatal exposure of DA, and remained irreversibly up until the maturation period.

Among multiple endpoints of the behavioral test battery we used, serious deviances in anxiety-related behaviors of group C (DA@14.5) and D (DA@17.5) mice were observed. Mice in those groups showed low performances in adaptations for novel circumstances, i.e., strange and broad area in OF test, beamish place in LD test, high and narrow space in EP test. Additionally, we also found severe impairment of learning and memory. Although the low performances of memory task have been reported in rats with prenatal DA exposure (Levin *et al.*, 2005),

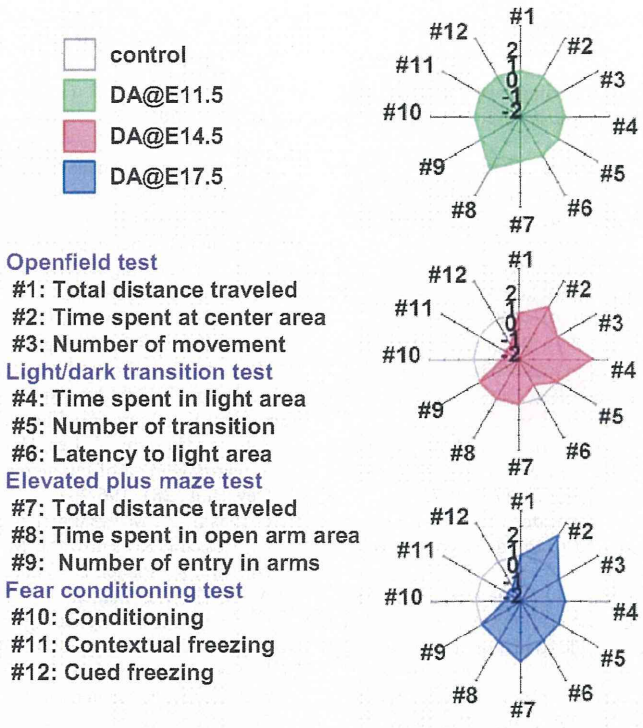

Fig. 7. Summary radar chart of the neurobehavioral battery test results. Radial axis indicates the direction (increase or decrease) of the deviation, and the p value of the endpoints compared to the control (+1 and −1, $0.01 <= p < 0.05$, +2 and −2, $p < 0.01$). Regular dodecagon of radius 0 indicates no deviation from control.

we showed serious deviances about affective (emotional) behaviors additional to severe memory deficit.

In conclusion, we clearly indicated that the disturbance against the adequate neural activity during developmental period when glutamate receptors became active have induced delayed memory defect and unnatural adoptive behaviors that became monitorable at the maturation period in mice. The responsible foci deduced from these behavioral disturbances are the limbic cortex and hippocampus. Our morphological findings are consistent with the interpretation. A combination of neurobehavioral and pathomorphological analysis was shown to be an effective method to assess delayed neurotoxic effects which dose not induce immediate organic brain damage and related symptoms after exposure. Having adopted the hypothesis that exogenous stimuli to neural signaling systems during the development of the brain can be a cause of delayed anomaly of higher brain function, stimuli toward systems other than glutamate receptors should also induce such anomaly of different targets and symptoms in concert with the distribution of the corresponding receptor(s) in the developing brain. Such data on other system would be reported elsewhere.

ACKNOWLEDGMENTS

The authors thank Mr. Yusuke Furukawa and Ms. Maki Otsuka for technical support. This study was supported by Health Sciences Research Grants H17- -Kagaku- 001 from the Ministry of Health, Labour and Welfare, Japan.

This peer-reviewed article is based upon a lecture presented at the 35th Annual Meeting of Japanese Society of Toxicology, June 2008 in Tokyo under the theme of "Children's Toxicology", June 2008 in Tokyo.

REFERENCES

Bondy, S.C. and Campbell, A. (2005): Developmental neurotoxicology. J. Neurosci. Res., **81**, 605-612.

Chandrasekaran, A., Ponnambalam, G. and Kaur, C. (2004): Domoic acid-induced neurotoxicity in the hippocampus of adult rats. Neurotox. Res., **6**, 105-117.

Cohen-Cory, S. (2002): The developing synapse: construction and

modulation of synaptic structures and circuits. Science, **298**, 770-776.

Dakshinamurti, K., Sharma, S.K., Sundaram, M. and Watanabe, T. (1993): Hippocampal changes in developing postnatal mice following intrauterine exposure to domoic acid. J. Neurosci., **13**, 4486-4495.

Fonta, C., Chappert, C. and Imbert, M. (2000): Effect of monocular deprivation on NMDAR1 immunostaining in ocular dominance columns of the marmoset Callithrix jacchus. Vis. Neurosci., **17**, 345-352.

Greer, P.L. and Greenberg, M.E. (2008): From synapse to nucleus: calcium-dependent gene transcription in the control of synapse development and function. Neuron, **59**, 846-860.

Gu, Q.A., Bear, M.F. and Singer, W. (1989): Blockade of NMDA-receptors prevents ocularity changes in kitten visual cortex after reversed monocular deprivation. Brain Res. Dev. Brain Res., **47**, 281-288.

Levin, E.D., Pizarro, K., Pang, W.G., Harrison, J. and Ramsdell, J.S. (2005): Persisting behavioral consequences of prenatal domoic acid exposure in rats. Neurotoxicol. Teratol., **27**, 719-725.

Luján, R., Shigemoto, R. and López-Bendito, G. (2005): Glutamate and GABA receptor signalling in the developing brain. Neuroscience, **130**, 567-580.

Manent, J.B., Demarque, M., Jorquera, I., Pellegrino, C., Ben-Ari, Y., Aniksztejn, L. and Represa, A. (2005): A noncanonical release of GABA and glutamate modulates neuronal migration. J Neurosci., **25**, 4755-4765.

Matsugami, T.R., Tanemura, K., Mieda, M., Nakatomi, R., Yamada, K., Kondo, T., Ogawa, M., Obata, K., Watanabe, M., Hashikawa, T. and Tanaka, K. (2006): Indispensability of the glutamate transporters GLAST and GLT1 to brain development. Proc. Natl. Acad. Sci. USA, **103**, 12161-12166.

Maucher, J.M. and Ramsdell, J.S.(2007): Maternal-fetal transfer of domoic acid in rats at two gestational time points. Environ Health Perspect., **115**, 1743-1746.

Miller, R.H. and Mi, S. (2007): Dissecting demyelination. Nat. Neurosci., **10**, 1351-1354.

Ooi, L. and Wood, I.C. (2008): Regulation of gene expression in the nervous system. Biochem. J., **414**, 327-341.

Pulido, O.M. (2008): Domoic acid toxicologic pathology: a review. Mar. Drugs, **6**, 180-219.

Rice, D. and Barone, S.Jr. (2000): Critical periods of vulnerability for the developing nervous system: evidence from humans and animal models. Environ. Health Perspect., **108**, 511-533.

Tanemura, K., Murayama, M., Akagi, T., Hashikawa, T., Tominaga, T., Ichikawa, M., Yamaguchi, H. and Takashima, A. (2002): Neurodegeneration with tau accumulation in a transgenic mouse expressing V337M human tau. J Neurosci., **22**, 133-141.

Tanemura, K., Ogura, A., Cheong, C., Gotoh, H., Matsumoto, K., Sato, E., Hayashi, Y., Lee, H.W. and Kondo, T. (2005): Dynamic rearrangement of telomeres during spermatogenesis in mice. Dev. Biol., **281**, 196-207.

Tatebayashi, Y., Miyasaka, T., Chui, D.H., Akagi, T., Mishima, K., Iwasaki, K., Fujiwara, M., Tanemura, K., Murayama, M., Ishiguro, K., Planel, E., Sato, S., Hashikawa, T. and Takashima, A. (2002): Tau filament formation and associative memory deficit in aged mice expressing mutant (R406W) human tau. Proc. Natl. Acad. Sci. USA, **99**, 13896-13901.

Tryphonas, L. and Iverson, F. (1990): Neuropathology of excitatory neurotoxins: the domoic acid model. Toxicol Pathol., **18**, 165-169.

Wiesel, T.N. (1982): Postnatal development of the visual cortex and the influence of environment. Nature, **299**, 583-591.

OPEN ACCESS Freely available online PLoS COMPUTATIONAL BIOLOGY

Structure of Protein Interaction Networks and Their Implications on Drug Design

Takeshi Hase[1☯], Hiroshi Tanaka[2☯*], Yasuhiro Suzuki[3], So Nakagawa[4], Hiroaki Kitano[5,6,7*]

1 Department of Bioinformatics, Medical Research Institute, Tokyo Medical and Dental University, Bunkyo-ku, Tokyo, Japan, **2** Department of Bioinformatics, Graduate School of Biomedical Science, Tokyo Medical and Dental University, Bunkyo-ku, Tokyo, Japan, **3** Department of Complex Systems Science, Graduate School of Information Science, Nagoya University, Nagoya, Aichi, Japan, **4** Center for Information Biology and DNA Databank of Japan, National Institute of Genetics, Mishima, Shizuoka, Japan, **5** Sony Computer Science Laboratories, Shinagawa, Tokyo, Japan, **6** The Systems Biology Institute, Minato, Tokyo, Japan, **7** Okinawa Institute of Science and Technology, Kunigami, Okinawa, Japan

Abstract

Protein-protein interaction networks (PINs) are rich sources of information that enable the network properties of biological systems to be understood. A study of the topological and statistical properties of budding yeast and human PINs revealed that they are scale-rich and configured as highly optimized tolerance (HOT) networks that are similar to the router-level topology of the Internet. This is different from claims that such networks are scale-free and configured through simple preferential-attachment processes. Further analysis revealed that there are extensive interconnections among middle-degree nodes that form the backbone of the networks. Degree distributions of essential genes, synthetic lethal genes, synthetic sick genes, and human drug-target genes indicate that there are advantageous drug targets among nodes with middle- to low-degree nodes. Such network properties provide the rationale for combinatorial drugs that target less prominent nodes to increase synergetic efficacy and create fewer side effects.

Citation: Hase T, Tanaka H, Suzuki Y, Nakagawa S, Kitano H (2009) Structure of Protein Interaction Networks and Their Implications on Drug Design. PLoS Comput Biol 5(10): e1000550. doi:10.1371/journal.pcbi.1000550

Editor: Andrey Rzhetsky, University of Chicago, United States of America

Received June 22, 2009; **Accepted** September 29, 2009; **Published** October 30, 2009

Copyright: © 2009 Hase et al. This is an open-access article distributed under the terms of the Creative Commons Attribution License, which permits unrestricted use, distribution, and reproduction in any medium, provided the original author and source are credited.

Funding: A part of this research is supported by Japan Science and Technology Agency (JST) through ERATO-SORST Program to HK. The funders had no role in study design, data collection and analysis, decision to publish, or preparation of the manuscript.

Competing Interests: The authors have declared that no competing interests exist.

* E-mail: kitano@sbi.jp (HK); tanaka@cim.tmd.ac.jp (HT)

☯ These two authors contributed equally to the article.

Introduction

There is a growing awareness that networks of protein interactions and gene regulations are the keys to understanding diseases and finding accurate drug targets [1]. With the increasing availability of genome-wide data including those on protein interactions and gene expressions, numbers of studies have been done on the structure and statistics of protein interactions and how diseased genes and drug targets are distributed over the network [2,3]. Understanding the topological and statistical properties of interaction networks and their relationships with lethal genes as well as currently identified drug targets should provide us with insights into robust and fragile properties of networks and possible drug targets for the future. We studied budding-yeast and human protein-protein interaction networks (PINs) to identify the architectural properties of network structures.

PINs have often been argued to be "scale-free" [4,5], which mostly means they have power-law frequency-degree distributions. However, this definition diverges from the original meaning of being scale-free in terms of the self-similarity of geometric properties of subject systems and there have been reports that claim such distributions are "more normal than normal"; thus, they are not considered to be particularly exotic by themselves [6]. In addition, there are different network topologies with different robustness and performance properties that maintain power-law distributions [7]. Therefore, it is very important to identify the architectural features of the network bearing the specific utilization of analysis results in mind. Our goal in this study was to identify the network topology of PINs and their relationship with lethal genes and possible drug targets so that the statistical likelihood of novel drug targets could be inferred.

A particularly interesting issue in the field of systems engineering, physics, and systems biology is the trade-off between the properties of robustness, fragility, and efficiency. Highly optimized tolerance (HOT) theory is a conceptual framework that can be used to explain this issue. Although a system conforming to HOT theory is optimized for specific perturbations and has highly efficient properties, such a system is extremely fragile against unexpected perturbations [8,9]. Doyle et al. [8] demonstrated that the Abline Internet2 router-level topology network conformed to HOT theory. Nodes in the Abline network with extremely high-degree nodes connect to a large number of low-degree nodes, while links between these high-degree nodes are suppressed and thus they do not form a core backbone for the whole network. A network having similar structures to the Abline network is defined as a HOTnet [8]. It would be very interesting to clarify whether PINs are HOTnets or not.

The two questions addressed in this paper are: (1) what is the global architecture of PINs? Do they follow the possible architectural features of scale-free networks created by preferential attachments or conform to HOT theory, and (2) are there specific statistical features for proteins that are likely to be drug targets? To

Author Summary

Genome-wide data on interactions between proteins are now available, and networks of protein interactions are the keys to understanding diseases and finding accurate drug targets. This study revealed that the architectural properties of the backbones of protein interaction networks (PINs) were similar to those of the Internet router-level topology by using statistical analyses of genome-wide budding yeast and human PINs. This type of network is known as a highly optimized tolerance (HOT) network that is robust against failures in its components and that ensures high levels of communication. Moreover, we also found that a large number of the most successful drug-target proteins are on the backbone of the human PIN. We made a list of proteins on the backbone of the human PIN, which may help drug companies to search more efficiently for new drug targets.

answer these questions, budding yeast and human PINs were used to analyze their structural properties using a series of analysis methods.

Results

Scale-free Network vs. Highly Optimized Tolerance Network: A series of analyses was carried out using budding yeast and human PIN data to identify the topological features of PINs.

In this study, we defined low-degree nodes as nodes with degrees of less than 5 because Han et al. [10] and Partil and Nakamura [11] defined hubs as nodes with degrees of more than 6. We then developed a method called moving stratification by degrees (MSD) to extract sub-networks consisting of hubs with specific degree distributions where indices such as average cluster coefficients would be computed (see Materials and Methods for details). The analyses revealed that the average cluster coefficient was very high for sub-networks consisting of hubs with degrees from 6 to 38, while it was very low for hubs with degrees of more than 39 in the yeast PIN (see Figure S1 and Table S1). Notably, for hubs with degrees of less than 38, the difference in cluster coefficients was generally significant between the yeast PIN and random network, while there were no significant differences in cluster coefficients for hubs with degrees of more than 39 (see Figure S1). Therefore, we defined middle-degree nodes as those with degrees from 6 to 38 and those with degrees of more than 39 as high. In the same manner, we defined middle- (from 6 to 30) and high-degree (more than 31) nodes in the human PIN (see Figure S2 and Table S2). Note that, when we used more stringent thresholds for middle- (from 10 to 50) and high-degree (more than 51) nodes, the results did not change essentially, i.e., the average cluster coefficient for middle-degree nodes was much higher than that for high-degree nodes (see Tables S3 and S4).

The analyses revealed three findings: (1) the network structure for middle-degree nodes (from 6 to 38 for yeast and from 6 to 30 for human PINs), and high-degree nodes (more than 39 for yeast and more than 31 for human PINs) has different structures, (2) middle-degree nodes are tightly connected and form a structure often called a "stratus", and (3) high-degree nodes do not connect, but connect with low-degree nodes, and form an "altocumulus" structure (Figures 1 and 2). Notably, we used more stringent thresholds for middle- (degrees from 10 to 50) and high-degree nodes (degrees more than 51), and found that changing the thresholds did not essentially affect the results (see Figure S3 and S4). These results suggests that PINs have an architecture where highly interconnected middle-degree nodes form a core backbone for the whole network and large numbers of low-degree nodes connect to high-degree nodes (see Figure 2). This architecture is a type of network that is suggested as a HOTnet, i.e., a network with HOT properties, also seen in the Internet router-level topology [8]. To further confirm this observation, we calculated a graph-theoretic quantity, $s(g)$, that defines the likelihood high-degree nodes will be connected to one another (see Materials and Methods for details). $S(g)$, a value normalized against s_{max}, indicates that networks with tightly interconnected high-degree nodes tend to be closer to 1.0, whereas networks with only sparsely interconnected high-degree nodes tend to be closer to 0.0 (see Materials and Methods for details). Doyle et al. reported randomly generated preferential-attachment-type scale-free networks had relatively high values such as 0.61, whereas a HOTnet exemplified by a network abstracted from an actual Abilene Internet2 router topology network had a value as low as 0.34 [8]. We found that the value of $S(g)$ for the yeast PIN was 0.25 and that of the human PIN was 0.38. Thus, we could conclude that PINs are HOTnets.

PINs are networks with a modular structure [12–14]. Here, modularity is defined as characteristics where there are fewer links

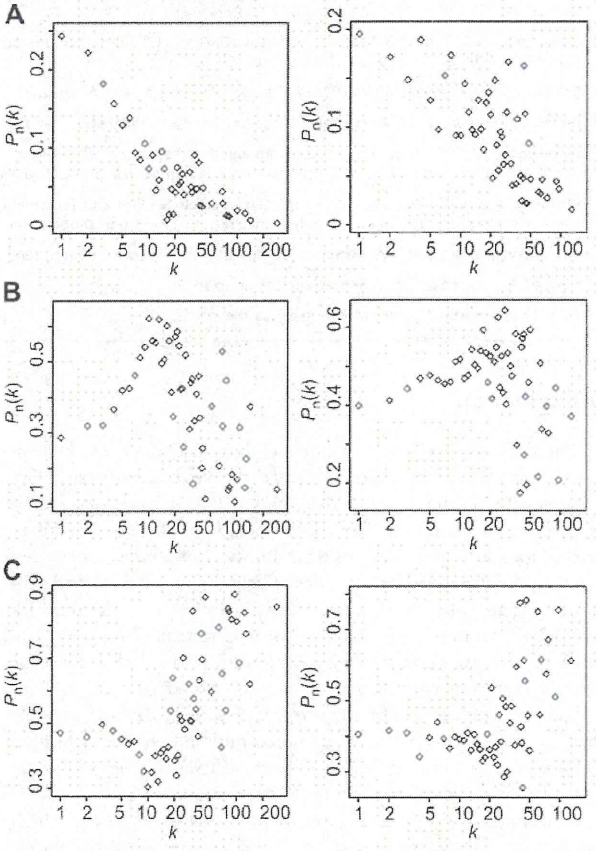

Figure 1. Degree dependent connectivity chart. $P_n(k)$ gives the probability that a link of a k-degree node is a link to a node in each sub-network of the yeast (left) and human (right) PINs. The value of $P_n(k)$ is calculated for a sub-network consisting of high-degree nodes, that consisting of middle-degree nodes, and that consisting of low-degree nodes. **(A)** Distribution of $P_n(k)$ for the high-degree sub-network. **(B)** Distribution of $P_n(k)$ for the middle-degree sub-network. **(C)** Distribution of $P_n(k)$ for the low-degree sub-network.
doi:10.1371/journal.pcbi.1000550.g001

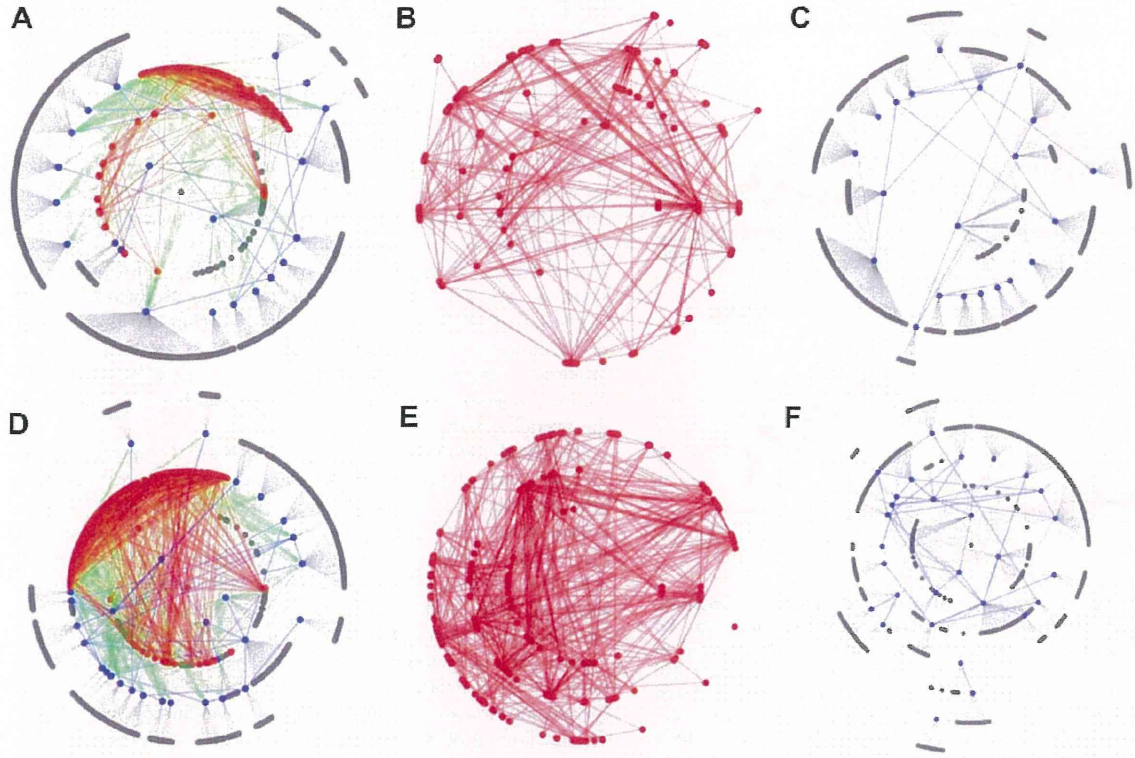

Figure 2. Cloud topology in yeast and human PINs. Grey, red, and blue nodes correspond to low-, middle-, and high-degree nodes. Grey, red, green, and blue links correspond to links between low- and high-degree nodes, those between middle-degree nodes, those between middle- and high-degree nodes, and those between high-degree nodes. For clarity, low- and middle-degree nodes that have no links to high-degree nodes have been omitted. **(A)** Altocumulus and stratus structures in the yeast PIN. **(B)** Stratus structure in the yeast PIN. **(C)** Altocumulus structure in the yeast PIN. **(D)** Altocumulus and stratus structure in the human PIN. **(E)** Stratus structure in the human PIN. **(F)** Altocumulus structure in the human PIN.
doi:10.1371/journal.pcbi.1000550.g002

between nodes with similar degrees. This only means there are limited links between high-degree nodes (hubs), whereas there are links between hubs and low-degree nodes. This is a feature that was also confirmed in this study (see Figure 2). Modularity in PINs implies that networks have two features [13]: First, functional units may be composed of many low-degree nodes that are directly connected to a hub node. Second, confusion between modules is avoided by avoiding direct connection between hubs. While there are arguments against this claim that hubs are tightly connected because they need to influence one another to achieve an integrated function for the whole system [15], analysis results indicate that such integration is most likely to take place via middle-degree nodes instead of high-degree nodes (see Figure 2).

The distribution of essential genes, synthetic genes, and other genes are shown in Figure 3. It is interesting to note that both essential genes and synthetic lethal genes have similar distributions. The average degree of essential proteins is 4.95 and that of synthetic lethal proteins is 4.40. However, the Wilcoxon rank sum test demonstrated that there is no statistical significance between them ($P = 0.334$). In either case, essential and synthetic lethal proteins are concentrated on middle-degree nodes and high-degree nodes. However, the average degree among synthetic sick genes is 4.07 and this is significantly lower than that among synthetic lethal genes ($P = 0.0015$). This means genes that have less severe impact are distributed toward regions with a lower-degree distribution.

Scale-richness: The power law distribution often characterized for scale-free networks only means that local frequency-degree distributions are independent of location along the degree axis, rather than self-similarity of network structures. However, Tanaka demonstrated that bacterial metabolic networks are scale rich in the sense there are different categories of metabolites and enzymes depending on the degree of nodes [16]. A group of nodes with high degree tends to be composed of currency molecules such as ATP and a group of nodes with low degree mostly consists of enzymes involved in specific cellular functions. In this study, we investigated if the frequency-degree distribution of proteins for each functional category exhibited the scale-rich characteristics reported by Tanaka. Figures 4 and S5 correspond to frequency-degree plots for proteins in different functional categories in the yeast PIN and the human PIN. The functional categories were assigned based on the GO slim ontology. As shown in the figures, the degree distribution patterns differ among functional categories. Moreover, proteins with different GO slim annotations have different average degrees (See Tables S5 and S6). Note that many functional categories have significantly higher (or lower) average degrees than the whole PINs (See Tables S5 and S6). These results suggest that the yeast and human PINs are scale-rich.

Drug Targets: Drug-target molecules are distributed over low- to middle-level degree nodes with higher probability on middle-degree nodes. Consistent with reports already published, the average degree among drug-target nodes (4.74) is higher than the average degree among all nodes (4.06).

The distribution of known drug targets is shown in Figure 5 and this is predominantly distributed to middle-degree nodes and

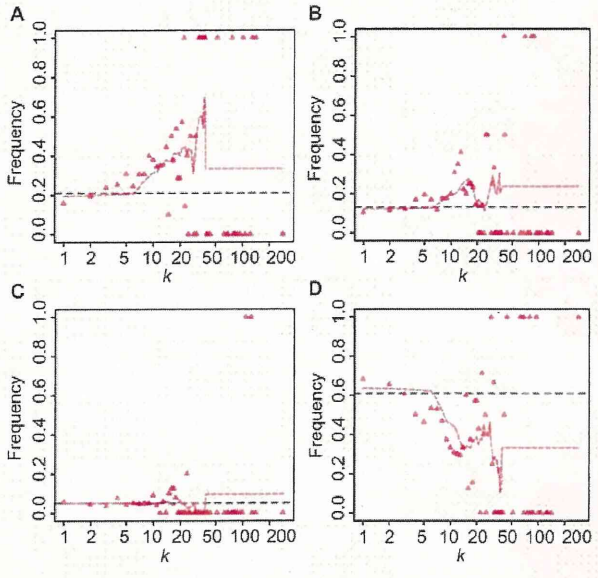

Figure 3. Degree distribution of essential proteins, synthetic lethal proteins, synthetic sick proteins, and proteins that do not belong to any of these (normal proteins). **(A)** Fraction of essential proteins to all proteins with degree k (red triangles). **(B)** Fraction of synthetic lethal proteins to all proteins with degree k (red triangles). **(C)** Fraction of synthetic sick proteins to all proteins with degree k (red triangles). **(D)** Fraction of normal proteins to all proteins with degree k (red triangles). Dashed lines in black give the probability that a randomly selected protein is essential, synthetic lethal, synthetic sick, or normal. Dashed lines in red represent fraction of essential, synthetic lethal, synthetic sick, or normal proteins to all proteins with degree from $k-5$ to $k+5$, when $k \leq 38$. When $k>38$, dashed lines in red represent fraction of essential, synthetic lethal, synthetic sick, or normal proteins to all proteins with degrees more than 38.
doi:10.1371/journal.pcbi.1000550.g003

mostly on backbone of the network. There are almost no drug targets for high-degree nodes. The distribution of drug targets for cancer and non-cancerous diseases are in sharp contrast. While the average degree of target nodes for cancer drugs was 7.82, the targets for non-cancerous diseases scored only 4.24 ($P=0.01$). Moreover, we found that the proportion of drug targets among low-degree proteins were similar to random expectation. Figure 6 shows distribution of drug targets marked on degree-rank plot. The drug target molecule that has highest degree is Src with 41 which is the target for drugs such as Dasatinib. Target molecules for anti-cancer drugs are shifted toward high degree nodes compare against average and non-anti-cancer drugs.

Discussion

A series of analyses revealed that both the budding yeast and human PINs are scale-rich and have HOT networks. There are extensive interconnections among middle-degree nodes that form the backbone of the network (see Figure 2). Most drug-target genes concentrate on middle-degree nodes and parts of low-degree nodes, but not on high-degree nodes. Interestingly, Feldman et al. (2008) [17] reported that genes harboring inherited disease mutations also concentrated on middle-degree nodes. Because of the potential lethality observed in budding yeast (Figure 3A) and reported high lethality in mouse knockout [2], high-degree nodes are unlikely to be preferred drug targets or genes with disease mutations. Since oncogenes tend to be high-degree nodes, they are less likely to be drug targets, or one has to accept major potential side effects. The fact that the degree distribution of cancer-drug targets is higher than that of non-cancer-drug targets is consistent with the report by Yao and Rzhetsky [18]. Since high-degree nodes are predominantly connected with low-degree nodes (Figures 1, 2, S3, and S4), the elimination of high-degree nodes is likely to affect large numbers of low-degree nodes. This may result in unacceptable side effects since a group of genes that bear certain functions may be made collectively dysfunctional. Detailed case studies are warranted to test and verify this possible interpretation. However, the average degree distribution of synthetic sick genes (4.07) is less than that of essential genes (4.95) and synthetic lethal genes (4.40). This implies that a drug design strategy to generate synergetic effects by targeting less important targets can be a reasonable option because each compound in such drugs can select targets that have less impact on the overall system alone.

We found that middle-level degree nodes are the optimal targets for therapeutic drugs. A similar observation was reported by Yao and Rzhetsky [18], although they measured the mean degree among drug targets. In this study, we investigated the degree distribution of drug targets in greater detail, because we measured a fraction of drug targets to all nodes with degree k as well as mapping drug targets on the network structure. It was clearly identified most of drug targets for drugs that are currently on the market are concentrated on middle degree nodes that are back bone of the network and low-degree nodes that tends to have specific function specific effects. One of novel findings here is that the distribution of drug targets for low-degree nodes is similar to random expectation, indicating that there are a certain number of low-degree drug targets. From these results, we can expect that the most advantageous targets for combinatorial drugs could be among low-degree nodes because these could have less severe impact on the overall system of the human body. This is consistent with the idea of "long-tail drugs"[19].

Are there any relationships between structures in molecular networks (i.e., scale-richness in PINs) and the properties of their underlying genome? Rzhetsky and Gomez [20] proposed a stochastic model describing the evolutionary growth of molecular networks. Their model predicts that, in a molecular network, the shape of the degree distribution will be similar to the shape of the distribution of domains in the genome. Actually, they showed that, in the case of the entire yeast PIN, both the degree distribution and the distribution of the domain followed a power law. Therefore, it might be interesting to see whether, for each functional category, the shape of the degree distribution was similar to that of the domain distribution, when the entire architecture of domains in genomes becomes available.

In this study, we assumed that the PINs represented all functions of genes. However, the PINs are just composed of binary protein-protein binding and proteins have other types of functions, such as catalyzing reactions with non-protein substrates. Therefore, PINs reflect a subset of the entire cellular function. This indicates that, if the complete picture for cellular protein functions could be considered, our conclusions from the PINs may diverge from what we presented here. Moreover, at present, the yeast and human PINs represent incomplete pictures of the actual entire PINs of these organisms. When data on all the actual entire PINs become available, we intend to examine all the actual entire PINs to see whether similar observations to those in this study can be made or not.

It is interesting to note that both PINs and the Internet topology are HOTnets. Many of the observed properties in Internet router topology may be applied to PINs as well. Such properties include